



Future climate change in the Northern Indian Ocean as simulated with a high-resolution regional earth system model

Dmitry V. Sein^{1,2} · Stanislav D. Martyanov² · Anton Y. Dvornikov² · William Cabos³ · Vladimir A. Ryabchenko² · Alok K. Mishra^{4,5} · Natalia Limareva⁶ · Evgenia Alekseeva⁷ · Daniela Jacob⁸ · Pankaj Kumar⁴

Received: 31 August 2022 / Accepted: 22 August 2023 / Published online: 15 September 2023
© The Author(s) 2023

Abstract

This study examines the future climate change in the South Asia region during 2070–2099 with respect to the historical period (1975–2004) under RCP8.5 scenario using a high-resolution regional earth system model. We found substantial changes in the key climatic parameters over the South Asia region including ocean biological productivity, however, the magnitude of response varies spatially. A substantial increase (> 2.5 °C) in the projected annual-mean sea surface temperature (SST) was found over the Indian Ocean with the highest increase (~ 3.4 °C) locally in the northern part of the Arabian Sea and in the Persian Gulf, SST changes being significant throughout the study area with 95% confidence level. The changes in the sea surface salinity showed strong spatial variability with the highest freshening over northern Bay of Bengal and highest salinity in the Persian Gulf followed by northern Arabian Sea. The amount of annual-mean precipitation will substantially increase over the eastern coast of the Bay of Bengal (up to 1.5–2.0 mm/day) and along the equator in the band 10° S–10° N (0.5–1.5 mm/day), while it will decrease over the western part of the Bay of Bengal and in the northern states of India (-0.5 to 1.0 mm/day). The most pronounced increase of precipitation rate in the future climate will occur over India (3–5 mm/day) and the eastern coasts of the Bay of Bengal (> 5 mm/day) during the monsoon period, and over the equatorial band (2–3 mm/day) during the post-monsoon period, with all precipitation changes indicated above being significant at 95% confidence level.

Keywords Regional climate modeling · Atmosphere-ocean coupling · Future climate change · Indian Ocean

1 Introduction

The land masses surrounding the Indian Ocean enclose some of the most densely populated areas on the planet. It is home to about a third of the world's population, which is especially vulnerable to extreme climate manifestations. For instance, the floods in the state of Assam in India in July–August 2020 caused the death of dozens of people and led to severe destruction that forced thousands of people to flee their homes. More than 480 people died in 2018 in the Indian state of Kerala during severe floods caused by unusually intensive rainfall during the monsoon season. In India, thousands of people lost their lives in 90 catastrophic floods between 2006 and 2015 compared to 67 floods during the decade before that, 1996–2005 (UNISDR 2016). Moreover, the frequency and severity of extreme occurrences over India are further increasing. To better understand the mechanisms implied in these events and improve our ability to predict their occurrence in the future, one should first study the possible changes in the ocean-atmosphere system in the future

✉ Dmitry V. Sein
dmitry.sein@awi.de

- ¹ Alfred Wegener Institute, Helmholtz Centre for Polar and Marine Research, Bremerhaven, Germany
- ² Shirshov Institute of Oceanology, Russian Academy of Sciences, Moscow, Russia
- ³ Universidad de Alcalá, Madrid, Spain
- ⁴ Department of Earth and Environmental Sciences, Indian Institute of Science Education and Research, Bhopal, India
- ⁵ Volcani Institute, Agricultural Research Organization, Rishon LeZion, Israel
- ⁶ North Caucasus Federal University, Stavropol, Russia
- ⁷ Odessa State Environmental University, Odessa, Ukraine
- ⁸ Climate Service Center Germany (GERICS), Hamburg, Germany

climate. A consistent way to do it is to use a climate model to assess the time-averaged changes in such a system in the future climate for the South Asia region.

The Indian Ocean variability is significantly controlled by the ocean-atmosphere interaction, and studying the related mechanisms seems a challenging though exciting task. To better understand the dynamics of the Indian Ocean and to track its current state to facilitate decision-making based on scientific knowledge, the Indian Ocean Observing System IndOOS was organized (Beal et al. 2019). However, due to the nature of observational data, it is not enough to fully understand the processes occurring in the climate system and to project changes in its state in the future. Various studies were attempted to understand the dynamic processes, circulation, and variability of the tropical Indian Ocean, including the Arabian Sea (AS) and the Bay of Bengal (BoB). In a pioneering work by McCreary et al. (1993) the Indian Ocean's dynamics and thermodynamics and its interaction with the atmosphere were studied using a simple 2.5-layer numerical model. The model reproduced well the general features of the ocean's thermodynamics properties. Still, it could not represent the detailed patterns of circulation, SST, etc. due to a relatively low horizontal resolution and the lack of the entire 3D representation of the ocean's dynamic processes. Jensen (2001) investigated the exchange of mass and salt between the AS and the BoB with an ocean model forced with the climatological atmospheric fields and found a significant influence of monsoon dynamics on the intrusions of saline water into the BoB. Estimates of surface freshwater runoff from the BoB to the tropical Indian Ocean were also reported by Sengupta et al. (2006). A modeling approach was used by Wiggert et al. (2006) to study biogeochemical variability in the tropical and northern Indian Ocean. They revealed the main mechanisms responsible for basin-wide spatiotemporal variability in ocean productivity such as iron limitation, Somali Current and Wyrтки Jet, Ekman pumping and westward propagating Rossby waves in the southern tropical region, and emphasized the need for additional studies based on the similar basin-wide approach to clarify the interplay between bioavailable iron distribution, physical–biological interactions and biogeochemical processes in the Indian Ocean. The research by Koné et al. (2009) highlighted the main features of phytoplankton bloom dynamics in the Indian Ocean during summer and winter periods. The variability of the mixed layer depth and its influence on the chlorophyll-a in the BoB was studied by Narvekar and Prasanna Kumar (2014). The comparative influence of air–sea forcings (winds, incoming shortwave radiation, and freshwater flux) was investigated by Srivastav et al. (2018), who suggested that wind plays a dominant role for the northern Indian ocean dynamical and thermodynamic processes. The ocean-atmosphere interaction and their

possible feedbacks in the region were also investigated in several studies focused on the Indian Ocean Dipole—an interannual mode of the tropical Indian Ocean variability that significantly affects the Southeast Asia climate (Li et al. 2002; Luo et al. 2007; Vinayachandran et al. 2002; Zheng et al. 2010). A comprehensive review of the Indian Ocean circulation, variability, ocean-atmosphere interactions, biogeochemistry, and corresponding intra-annual cycles was reported by Phillips et al. (2021). Authors emphasized the important impact of small-scale processes on the large-scale properties of the ocean, as well as the importance of ocean-atmosphere coupling in modeling studies.

Under climate change, the rapid warming of the Indian Ocean and ocean acidification are expected, likely leading to increased ocean extremes and hazards and severe threats to the marine ecosystem and devastating and long-lasting biological impacts. A reduction in ocean productivity in the northern part of the Indian Ocean and its connection with ocean warming over the last decades was reported by Roxy et al. (2016). Their findings demonstrated that the rapid warming of the ocean's surface layer during the past century had led to a 20% decrease in phytoplankton over the last 60 years due to enhanced stratification and thus decreased nutrient supply from the deep ocean. Other climate projections also showed a further decrease of ocean primary production in the future, the northern Indian Ocean being one of the regions with the most significant drop in ocean primary production (Bopp et al. 2013; Laufkötter et al. 2015; Steinacher et al. 2010). Thus, improving the predictive skill of ocean models is crucial for climate and Indian monsoon prediction and for improving the management of marine living resources and climate services to provide the foundation for informed decision-making. Climate change necessitates concerted action, and it should serve as a spur for the resurrection of the Indian Ocean Rim Association. Thus, reliable science-based tools are needed to assess the characteristics of the future climate and its impact on the frequency and severity of extreme weather events.

Nowadays, the main tools for studying the projected state of the future climate are numerical models including Atmosphere and Ocean General Circulation Models (AGCMs and OGCMs), and also global Earth System Models (ESMs). Global ESMs produce a lot of 3D state variables describing the ocean and atmosphere dynamics and composition. It makes the running and output of these models very 'heavy' in terms of computational time and data storage capacity required for carrying out the simulations and saving the results. Furthermore, if one needs to assess the climate change scenarios in any particular area on Earth, then the refinement of a computational grid (compared to general global coarse-resolution models) is required in order to correctly represent regional features such as coastline, islands, mountains, etc. In this respect, Regional Earth

System Models (RESMs), adequately tuned for a specific region of the Earth, are tools aimed at this particular purpose—to study regional features at the cost of neglecting the feedback between considered regional model's domain and outer domain. RESMs include components of the climate system other than ocean and atmosphere that allow to study some climatic feedbacks that cannot be studied by coupled ocean-atmospheric regional models. A comprehensive review of climate phenomena and processes in the Indian Ocean was given by Schott et al. (2009), where authors emphasize the need for numerically and physically improved models, combined with observations, to make future climate projections robust and reliable. Multi-model projections of precipitation in South and Southeast Asia based on coupled ESMs and a good review of the RESM's development progress were reported in recent studies (Supari et al. 2020; Tangang et al. 2020; Kumar et al. 2022a, b). For instance, Supari et al. (2020) examined the projections of precipitation extremes for the period 2081–2100 in Southeast Asia and showed that under the RCP8.5 scenario the heavier precipitation will occur over a wider area compared with the RCP4.5 scenario. Analyzing the results of multi-model simulations, Tangang et al. (2020) found that the mean rainfall intensity distribution will not be homogeneous both in space and time throughout the 21st century. Moreover, a significant uncertainty in precipitation projections was found among the member models.

Indian summer monsoon variability was investigated by Di Sante et al. (2019), Mishra et al. (2021a) by means of coupled RESMs RegCM-ES and RegCM-MITgcm, respectively. It was demonstrated that the air-sea feedback implemented in the coupled models enhanced the quality of the Indian summer monsoon rainfall simulation, as well as improved the results of simulation of wind speed and SST in the AS and the BoB. Similar results were earlier reported by Ratnam et al. (2009), who used the RegCM3-ROMS regional coupled model to simulate the Indian summer monsoon and who showed that the two-way coupled modeling system simulates the main features of the Indian monsoon much better compared to atmosphere-only model due to taking into account corresponding feedbacks between the SST and convective processes in the atmosphere. The importance of the two-way coupling between the ocean and the atmosphere for more realistic simulation of the Indian summer monsoon was also emphasized by Samala et al. (2013) on the basis of WRF-ROMS coupled model. Mishra et al. (2021b) demonstrated that the increase of a coupled model's horizontal resolution improved the results of monsoon simulation in the CORDEX-South Asia domain.

The present study is aimed to assess the changes in key parameters of the ocean-atmosphere system in the future climate for the South Asia region using state-of-the-art high-resolution RESM developed by Sein et al. (2022).

This RESM implements a global ocean component and a regional atmosphere component. Using this coupled model is advantageous compared to fully global ESMs because we can implement a higher spatial horizontal resolution in the atmospheric model. It allowed us to better reproduce spatial distribution of simulated fields by better taking into account such regional features as orographic-induced precipitation. Besides, the presence of a marine biogeochemical module allowed us to explicitly take into account the impact of the explicit marine biogeochemical light absorption on the simulated climate. Particular attention is paid to changes in ocean characteristics, including their validity and explanation of the causes of the most significant changes. This will contribute to the detection of weaknesses in models of the Earth's climate system and their further improvement.

The layout of the paper is as follows. Section 2 briefly describes the coupled modeling system used in this study. The model results and related discussion are presented in Sect. 3. In Sect. 4, we discuss the comparison of our results with prior relevant studies including CMIP5 and CMIP6 projections. Finally, Sect. 5 concludes the main findings of the study.

2 Methods

In the present study, we used the RESM ROM (Sein et al. 2015), which consists of the global Max Planck Institute Ocean Model—MPIOM (Jungclaus et al. 2013; Marsland et al. 2003), the Regional Atmospheric Model—REMO (Jacob 2001), the Hamburg Ocean Carbon Cycle Model—HAMOCC (Ilyina et al. 2013), and the Hydrological Discharge Model—HD (Hagemann and Dümenil 1997). All of the components were linked to each other via the OASIS coupler. The coupling frequency was three hours, while the forcing was updated each six hours.

The ocean component of ROM is global, whereas the atmospheric model is regional and is fully dynamically coupled with the ocean model only inside the South Asia CORDEX domain (<https://www.cordex.org>, Fig. 1a). Outside the coupling region, MPIOM calculates heat, freshwater, and momentum fluxes from the atmospheric fields taken from the same global model used for REMO boundary conditions. In the simulations analyzed here, the driving model MPI-ESM-LR was used both for lateral boundary conditions for REMO and for calculation of the atmospheric forcing for MPIOM outside the coupling subregion. The horizontal and vertical resolution of the atmospheric model inside the coupling domain was 25 km and 31 hybrid levels, respectively. The variable horizontal resolution of the ocean model inside the coupling domain ranged from 23.3 to 24.5 km. MPIOM employed 40 vertical z-coordinate levels with the following thicknesses (in

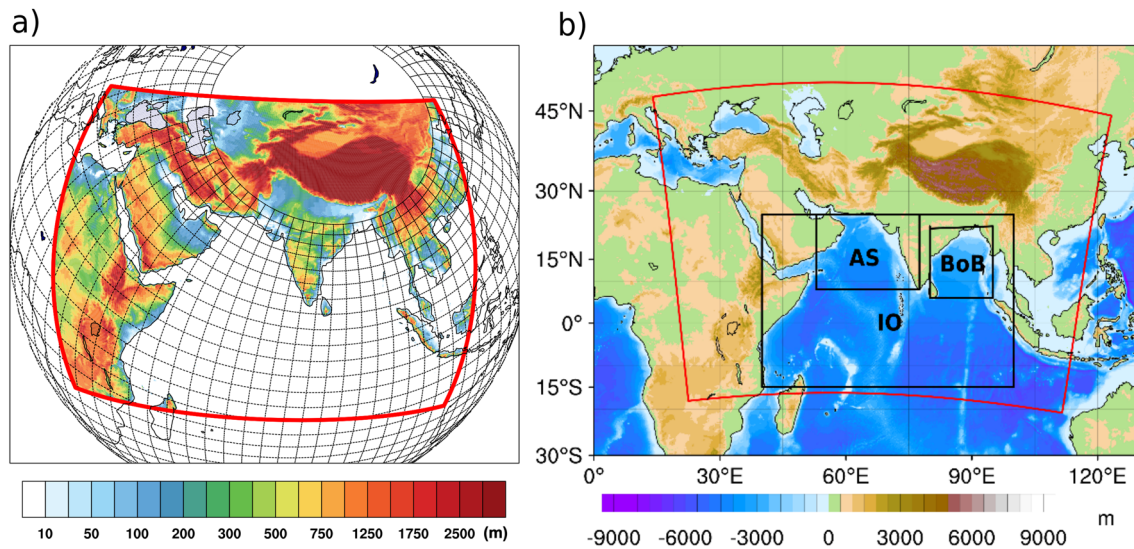


Fig. 1 **a** South Asia CORDEX domain as implemented in the current ROM configuration. The red frame shows the coupled ocean-atmosphere domain. The black lines show the global curvilinear grid of the ocean model (every 12th line is shown). **b** Specific areas in the model domain. The red square is the South Asia CORDEX domain. The

black squares inside denote the following regions used in the analysis: IO (northern part of the Indian Ocean, 40°–100° E, 15° S–25° N), AS (Arabian Sea, 53°–77.5° E, 8°–25° N), and BoB (Bay of Bengal, 80°–95° E, 6°–22.5° N). Color scale represents orography in both figures

meters): 16, 10, 10, 10, 10, 10, 13, 15, 20, 25, 30, 35, 40, 45, 50, 55, 60, 70, 80, 90, 100, 110, 120, 130, 140, 150, 170, 180, 190, 200, 220, 250, 270, 300, 350, 400, 450, 500, 500, 600. The model grid and parameters in the current study are identical to those used in the recent study by Sein et al. (2022). These coupled model's horizontal resolutions, for both ocean and atmosphere, are close to those implemented in other regional coupled models for Southeast Asia (25 km), e.g., by Supari et al. (2020) and Tangang et al. (2020).

Previously, we reported the results of the thorough verification of ROM and assessed the influence of different parameterizations of light attenuation in water upon physical and biogeochemical characteristics of the ocean and, through the ocean-atmosphere feedback, upon atmospheric dynamics, during the climatic period 1975–2004 (Sein et al. 2021, 2022). As a result, it was demonstrated that taking into account the impact of marine biogeochemical variability upon the attenuation of the solar short-wave radiation (SWR) in the water (Gröger et al. 2013) leads to a decrease of SST compared to the simulation with a constant light attenuation coefficient set equal to 0.06 m^{-1} (Jerlov 1976; Paulson and Simpson 1977). Furthermore, the ocean mixed-layer depth in the numerical experiment with full marine biogeochemical variability's impact was shown to be in a better agreement with available observations, along with better simulation of atmospheric precipitation.

Thus, having completed the ROM's verification for the past climatic period (1975–2004) and shown its ability to realistically simulate the main regional climate features in South Asia, in the current study we investigated the future

climate for the 2070–2099 period. To this end, we performed a simulation for the future South Asia climate under the RCP8.5 scenario taking into account the impact of the SWR absorption in the water column by explicitly-modeled phytoplankton. A corresponding influence of the SWR absorption on the water temperature (Gröger et al. 2013) and its feedback on heat and moisture flux between the ocean and the atmosphere was taken into account. Thus, due to spatial and temporal variability of modeled phytoplankton concentration, its aforementioned impact on water temperature was also spatially- and temporally-variable.

As stated in the study by Sein et al. (2022), after 100 years of spin-up, we carried out a simulation from 1920 to 2005 forced by the global MPI-ESM-LR CMIP5 historical run. Then, for this study, the model was further run for the 2006–2099 period forced by the fields from a MPI-ESM-LR simulation under the RCP8.5 scenario. We note that MPI-ESM-LR is among the best models that not only effectively estimates the mean climate but also the extremes globally (Sillmann et al. 2013). It has better mass and energy flow than other CMIP5 models (Vázquez-Patiño et al. 2020), better decadal prediction of precipitation, SST and 2-meter temperature (Purwaningsih and Hidayat 2016) even at a catchment level (Hossain et al. 2022) and is efficient in simulating global tropical cyclones (Shen et al. 2021). Over the CORDEX South Asia domain, MPI-ESM-LR has better simulation of East Asian Summer Monsoon (Guo et al. 2016) and better wind simulation (Lakku and Behera 2022). According to Sperber (2013), MPI-ESM-LR typically performs well

in simulations of the Indian Summer Monsoon and is a viable candidate for downscaling in the Indian Ocean region (McSweeney et al. 2015). Considering this high performance in simulating different spheres of Earth components, we chose MPI-ESM-LR as the model providing the forcing data.

ROM simulations of the past climate (1975–2004) of the South Asia CORDEX domain were previously presented and validated (Sein et al. 2022; Kumar et al. 2022a, b). It was shown that the regional ROM's setup was able to successfully reproduce the current climate of this region. In order to be consistent with those earlier results, in the present study we used the same seasonal periods which are defined by the India Meteorological Department based on the monsoon activity in the northern part of the Indian Ocean:

- DJF: December–February (winter season, north-east winds);
- MAM: March–May (pre-monsoon season);
- JJAS: June–September (monsoon season, south-west winds);
- ON: October–November (post-monsoon season).

We note that the base period 1976–2005 is commonly used as a reference period for climate studies because a 30-year period represents a period of relative stability in global temperature and weather patterns. It is also a period that is well documented by the World Meteorological Organization (WMO). Still, instead of taking the 1976–2005 period, in the current study we took the 1975–2004 period assuming that the shift in one year would not significantly change the results, but in this case the results obtained in the current study are fully consistent with those reported by Sein et al. (2022) where the same climatic period 1975–2004 was used for the verification of ROM and for the analysis of simulations.

The RCP8.5 scenario is one of several scenarios developed by the Intergovernmental Panel on Climate Change (IPCC) to model future greenhouse gas emissions and their impact on the climate. The RCP8.5 is a high emissions scenario that assumes that global emissions of greenhouse gasses will continue to rise throughout the 21st century. It is considered a “business as usual” scenario, meaning that it assumes no significant changes in human behavior or policies to reduce greenhouse gas emissions. The RCP8.5 was chosen in the current study, as well as in the previous study by Sein et al. (2022), because it gives the strongest climate change signal, allowing us to identify more clearly the impact of the feedback of the ocean marine biogeochemical variability on the climate change signal.

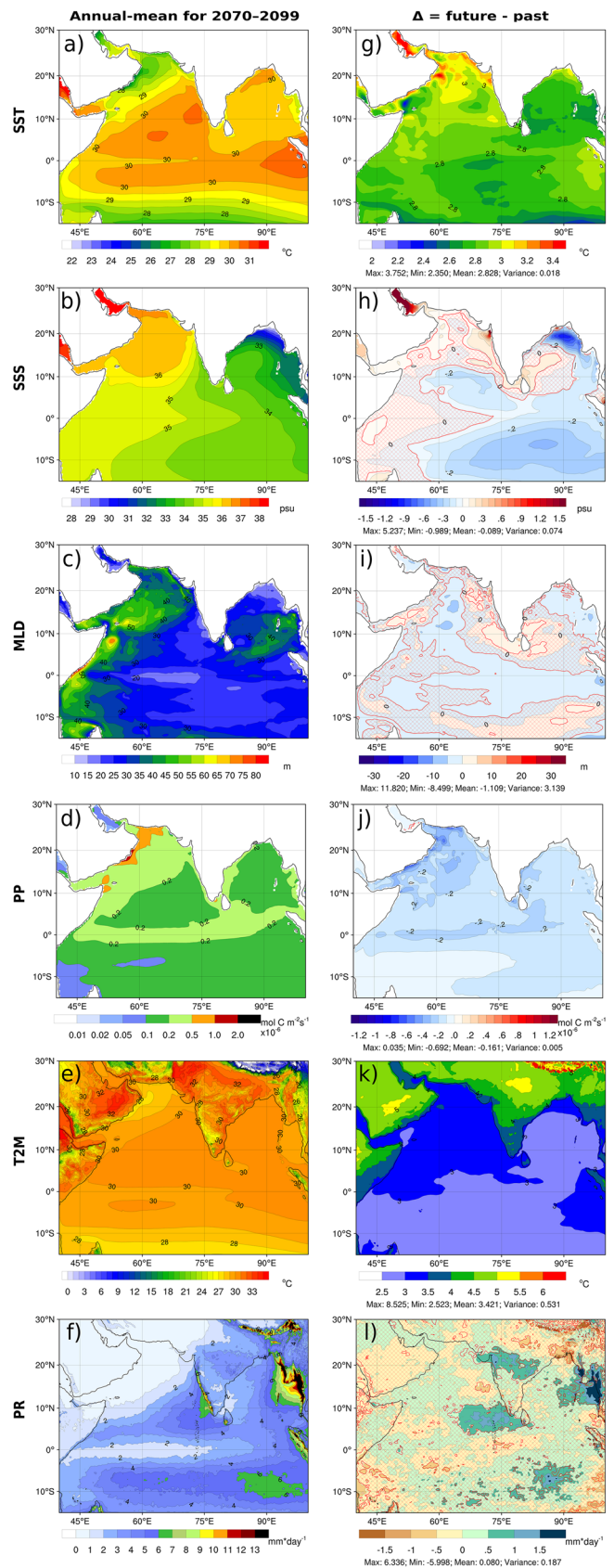
3 Results and discussion

In the following sections, we compared the past (1975–2004) and future (2070–2099) simulated South Asia climates to determine the corresponding changes in the ocean-atmosphere system's key parameters. The spatial distributions of sea surface temperature (SST), sea surface salinity (SSS), mixed-layer depth (MLD), depth-integrated phytoplankton primary production (PP), 2 m air temperature (T2M), and total precipitation rate (PR) were examined. Additionally, we also assessed the climatic intra-annual variation of these characteristics for the two periods considered in different areas of the model domain, namely in the AS and in the BoB.

Figure 2 shows the annual-mean modeled SST, SSS, MLD, PP, T2M and PR distributions for the future climate and the differences (Δ) between the future and past climatic periods (future–past)

A brief look at Fig. 2 emphasizes the main features of the simulated future climate change consequences in the considered area. According to our projection, SST in the northern part of the Indian Ocean will significantly increase in the future climate, while biological productivity will decrease. In general, the Arabian Sea shows north–south gradient of SST, having northward decreasing SST partly attributed to the northward deepening of MLD. Similarly, the northward increasing SST over the BoB is partly associated with a shallowing MLD as a result of increased freshwater flux and precipitation. This SST pattern might also be associated with atmospheric processes (heat fluxes) and small-scale ocean processes which are beyond the scope of this study. The non-uniform spatial distribution of SST in the Arabian Sea may be caused by a spatially-varying sensible heat flux between the sea and heated air transported from the south-west from Africa and Arabian Peninsula. Figure 2 shows that the 2 m air temperature (T2M) in these regions will rise considerably in the future climate according to ROM projection. In the northern part of the Indian Ocean, the annual-mean SST increase (Δ SST) will be 2.7–3.2 °C almost everywhere by the end of this century compared to the end of the last century. The main feature of the Δ SST spatial distribution is its larger values of 2.8–3.2 °C in the AS, in the northern part of which and in the Persian Gulf reaching 3.4 °C, compared to the BoB where Δ SST values reach 2.7–2.8 °C. The reason for this difference is a strong increase in 2 m air temperature (Δ T2M) over the Arabian Peninsula and Somalia: up to 5.5 °C for annual averages (Fig. 2) and up to 6.5 °C during the south-west monsoon period (JJAS), which leads to increased Δ T2M values over the AS compared to the BoB during the monsoon (JJAS) and autumn post-monsoon (ON)

Fig. 2 (Left column): Annual-mean modeled SST (a), SSS (b), MLD (c), PP (d), T2M (e) and PR (f) for the future (2070–2099) climate. (Right column): The differences (Δ) between the future and past climatic periods for each variable (future–past, g–l). Areas of statistically nonsignificant values are cross-hatched with red lines. The statistical significance for the differences Δ was calculated using Student’s *t* test at confidence interval of 95%. In figures where there is no cross-hatching, this means that all values are statistically significant



periods (Fig. 6). Based on our results, the highest spatial variation in changes of SST was found over the northern AS, with the small patches of local maximum changes. The overall range of SST change assessed with ROM is consistent with the previously reported studies using CMIP5 models, which was expected. Any regional model is, in general, focused towards the regional variability or changes due its capability of resolving the regional scale processes at higher resolution. Compared to previous studies, the horizontal resolution of ROM is higher than that of other coupled AOGCMs previously implemented for similar studies in that region (e.g., Krishnan et al. 2020). The benefits of using a regional model ROM with higher spatial resolution and specifically tuned for the CORDEX-SA region are discussed in Sect. 4 where we show and discuss in detail the intercomparison between ROM results and simulations carried out with models with coarser spatial resolution.

Based on ROM's results, the most striking decrease of ocean primary production (PP) in the future climate will occur in the AS, which is consistent with regions of prominent temperature increase. This result is in accordance with other previous studies, in which the decline of ocean primary production was discussed using observational data by Roxy et al. (2016) and model projections of future climate by Bopp et al. (2013), Laufkötter et al. (2015), Steinacher et al. (2010), the northern Indian Ocean being one of the regions with the most significant drop in ocean primary production. As expected, the 2 m air temperature will rise significantly in the future, especially above land. Considering the annual-mean spatial pattern, the difference between the two climatic periods reaches up to 5.5 °C in northern India and Arabian Peninsula, while it is 2.5–3.5 °C over the northern Indian Ocean. A comparatively higher increase in air temperature over land than in the surrounding ocean will strengthen the moisture-laden wind from the AS and BoB to Indian land region as a result of the increased land-sea pressure gradient. According to our simulations, the amount of annual-mean precipitation will substantially increase over the eastern coast of the BoB (up to 1.5–2.0 mm/day) and along the equator in the band 10° S – 10° N (0.5–1.5 mm/day), while it will decrease over the western part of the BoB and in the northern states of India (–0.5 to 1.0 mm/day). The main changes in SSS in the future climate will occur in the northern part of the BoB (up to –0.9 ppt), along the southern tropical band 0–15° S (circa –0.2 to 0.4 ppt), and in the Persian Gulf. The SSS decrease in the tropical band can be explained by the increased precipitation in this region in the future climate, while the increased salinity in the Persian Gulf is a consequence of enhanced evaporation. As for the northern BoB and the corresponding drop in SSS, the model results did not show any significant increase in precipitation, or a

drop in SST leading to a reduced evaporation rate. On the contrary, the model results showed that the precipitation rate in the northern part of the BoB will decrease in the future climate (Fig. 2). All these circumstances suggest that the above-mentioned pronounced SSS decrease in this area may be linked with the altered river runoff in the future climate. Figure 3d shows the simulated climatic intra-annual time-series of the total freshwater river runoff into the BoB for the two climatic periods considered. A slight increase in the river runoff compared to the past climate occurs at the end of the summer monsoon period. Nevertheless, it can hardly be fully responsible for the significant SSS decrease in the northern BoB. But, combined with a specific circulation pattern, which can hinder the free transport of riverine waters to the south in the future climate, the freshening of this area may still be plausible. To check this hypothesis, we calculated the changes of modeled current velocities in the upper ocean layer. Figure 3 shows that circular surface currents in the northern BoB will intensify in the future climate, with two gyres of the opposite rotation direction being the main part of this new circulation pattern (Fig. 3a). The first gyre, located in the northernmost part of the BoB, has the anticyclonic rotation, and the second gyre, located to the south from the former, is of the cyclonic rotation. Their combined effect leads to the local circulation that, to some degree, traps the waters freshened by the riverine runoff in the top of the BoB by means of the recirculation of that water. This new circulation pattern with two gyres in the northern part of the BoB is even more distinct when analyzed not at an annual but at a seasonal time scale, the monsoon and post-monsoon seasons (JJAS and ON) being the periods when, according to ROM's projection, the circulation driven by these gyres is the most intense (Fig. 3b and c), which also coincides with the maximal river runoff throughout the year in this region (Fig. 3d). Comparison of this result with those obtained with other models is given in Sect. 4.

The simulations also showed that there will be no distinct and uniform trend in the change of the MLD in the northern part of the Indian Ocean in the future climate. Among the main features of the modeled MLD for the future period, we can highlight the decrease of the annual-mean climatic MLD in the equatorial band by 10–15 m, in the BoB by 8–15 m, and in the AS by 6–10 m (Fig. 2). Still, in the areas located to the east of the Arabian Peninsula and the Somalia coast, the annual-mean MLD will increase in the future climate by about 8–10 m compared to the period 1975–2004.

Besides the mentioned changes in horizontal distribution, the vertical structure of water masses in the considered region, according to ROM simulations, will also be altered in the projected future climate. The vertical profiles of annual-mean spatially-averaged water temperature and salinity in different areas of the northern Indian Ocean are

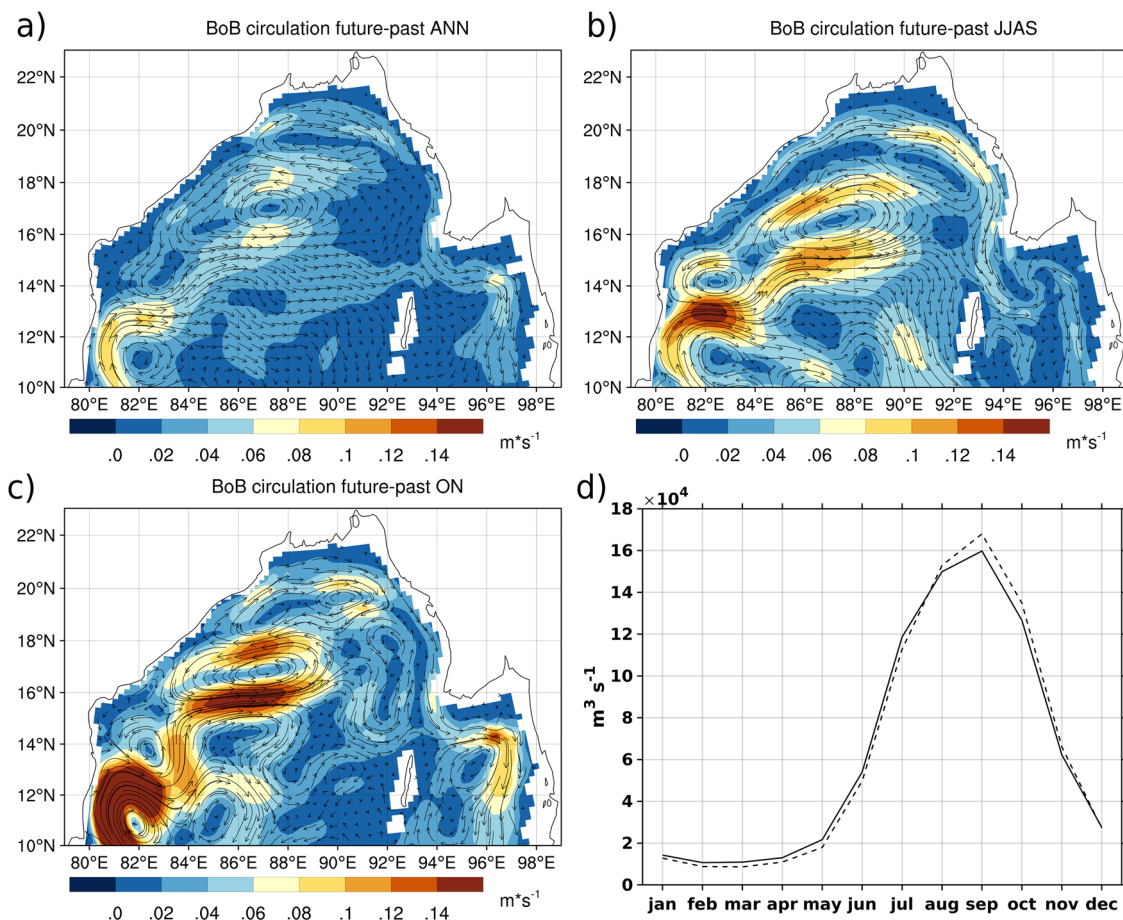


Fig. 3 Annual-mean (a) and seasonal-mean (b, c) modeled current velocity difference in the upper ocean layer between the climatic periods 1975–2004 and 2070–2099. **d** Simulated climatological annual

cycle of total freshwater river runoff into the BoB for the periods 1975–2004 (solid line) and 2070–2099 (dashed line)

shown in Fig. 4. The locations of the regions is shown in Fig. 1b and consist of: the northern part of the Indian Ocean, 40°–100° E, 15° S–25° N (IO); Arabian Sea, 53°–77.5° E, 8°–25° N; and the Bay of Bengal, 80°–95° E, 6°–22.5° N. The AS and the BoB regions were selected because the hydrological regimes of the AS and the BoB are very different. This is due to the river runoff into the BoB that is significantly larger than that in the AS. Also, the BoB is shallower than the AS, and the latter is affected by the summer monsoon to a greater extent than the BoB. Based on such spatial averaging, it is easier to track the future changes in key oceanic and atmospheric parameters in the regions of interest.

As follows from Fig. 4, the annual-mean water temperature difference between the two climatic periods is maximal at the surface and gradually decreases with depth, and almost vanishes at a depth of 300 m. The same cannot be said about salinity, though a somewhat SSS decrease in the BoB, and in the entire northern part of the Indian Ocean, is evident. Below the depth of 50–75 m, some increase of

salinity occurs in the projected future climate in all spatially-averaged regions considered. Still, this increase is much less compared to the surface salinity change, at least for the entire domain (IO). Overall, it can be concluded that in the projected future climate the water temperature's changes will be more pronounced than the salinity changes in terms of the depth of affected ocean layers. Both temperature and salinity changes in the future climate will lead to enhanced water stratification and vertical stability of the upper ocean layers, thus hindering the vertical turbulent mixing and nutrient supply to the surface, which results in decreasing of the ocean phytoplankton primary production in the northern part of the Indian Ocean (Fig. 2). The enhanced vertical stratification in the upper ocean layers in future climate is presented in Fig. 5 by means of plotting both climatic annual-mean Brunt-Väisälä frequency and vertical shear stress calculated from the model results for the 1975–2004 and 2070–2099 periods. The vertical distribution of shear stress for the period 2070–2099 does not show any significant changes in the water column compared with the

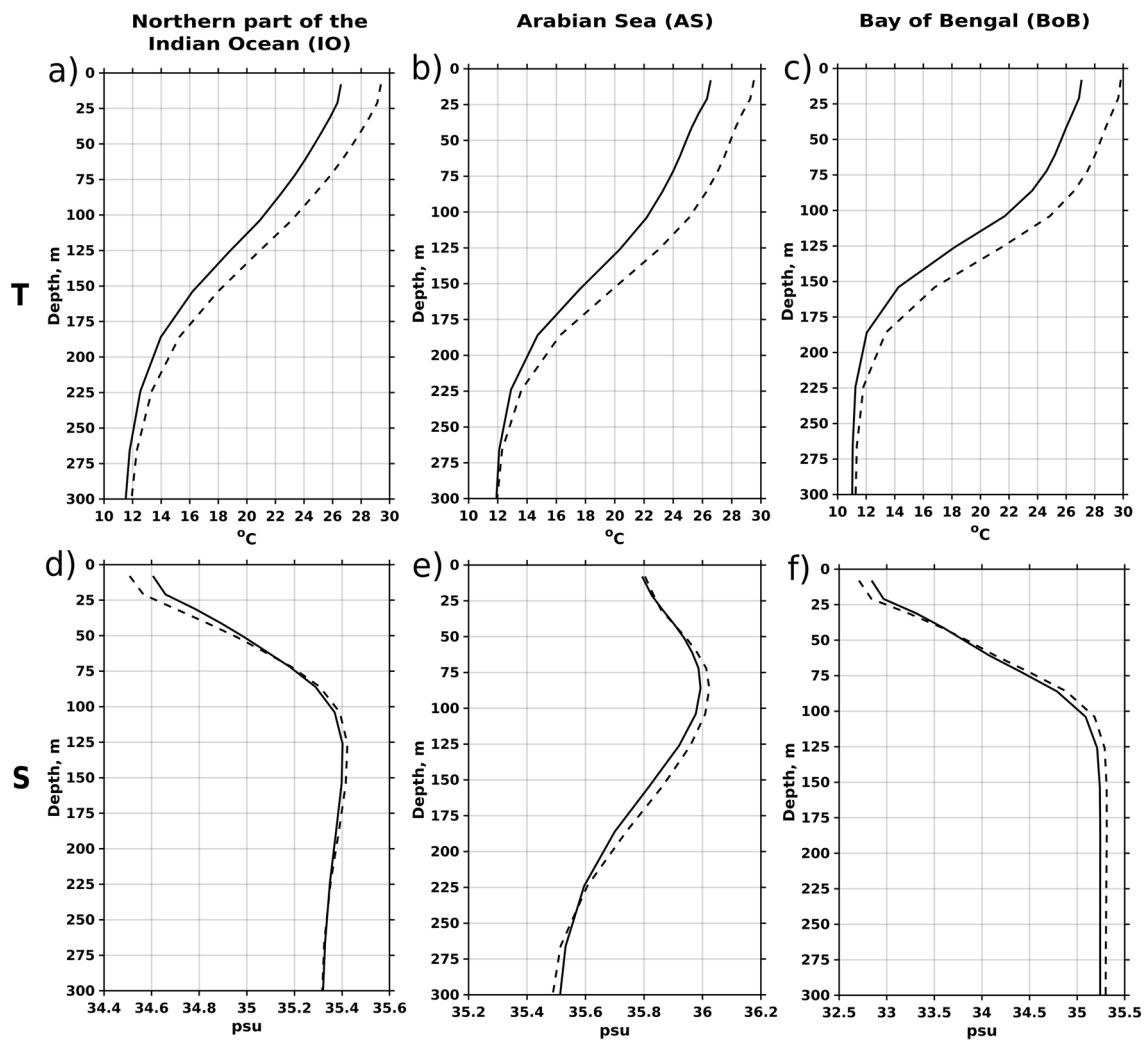


Fig. 4 Vertical profiles of modeled climatic annual-mean water temperature (a–c) and salinity (d–f) for the periods 1975–2004 and 2070–2099. IO denotes the northern part of the Indian Ocean, AS

Arabian Sea, *BoB* Bay of Bengal (see Fig. 1 for the exact locations of these regions). Solid line is for 1975–2004, dashed line is for 2070–2099

1975–2004 climatic period, while Brunt-Väisälä frequency demonstrates considerable increases in the upper 300 m. This result is in accordance with those reported earlier (e.g., Bopp et al. 2013; Laufkötter et al. 2015; Roxy et al. 2016; Steinacher et al. 2010).

The northern Indian Ocean region is characterized by a robust seasonal variability associated with monsoon dynamics. Therefore, it seems reasonable to examine in more detail the corresponding seasonal changes of the previously analyzed annual-mean characteristics between the two climatic periods. However, we confined the analysis of the climatic seasonal variations by considering only SST, T2M, PR and PP, presenting the corresponding difference between the two climatic periods as Δ SST, Δ T2M, Δ PR and Δ PP (Figs. 6 and 7). Regarding the differences between future and past seasonal climatic SSS (Δ SSS), though there

exists some variability of Δ SSS throughout the climatic seasons, the qualitative pattern of Δ SSS distribution (not shown) still resembles the one typical for the annual-mean climatic Δ SSS distribution shown in Fig. 2.

In all climatic seasons, there will be warming all over the study region in the projected future climate according to ROM simulations. However, these changes showed strong spatio-temporal variability. The most robust warming ($\sim 7^\circ\text{C}$) in the future will take place over the high mountain regions (the northern side of the Himalayas and the Tibetan Plateau) during winter, while during the monsoon season the highest warming ($\sim 5\text{--}6^\circ\text{C}$) will occur over the Arabian Peninsula and eastern Africa. The spatial distribution of the changes between the future and past climate is strongly influenced by the orographic features. The highest (lowest) warming over Himalayas and the Tibetan Plateau during

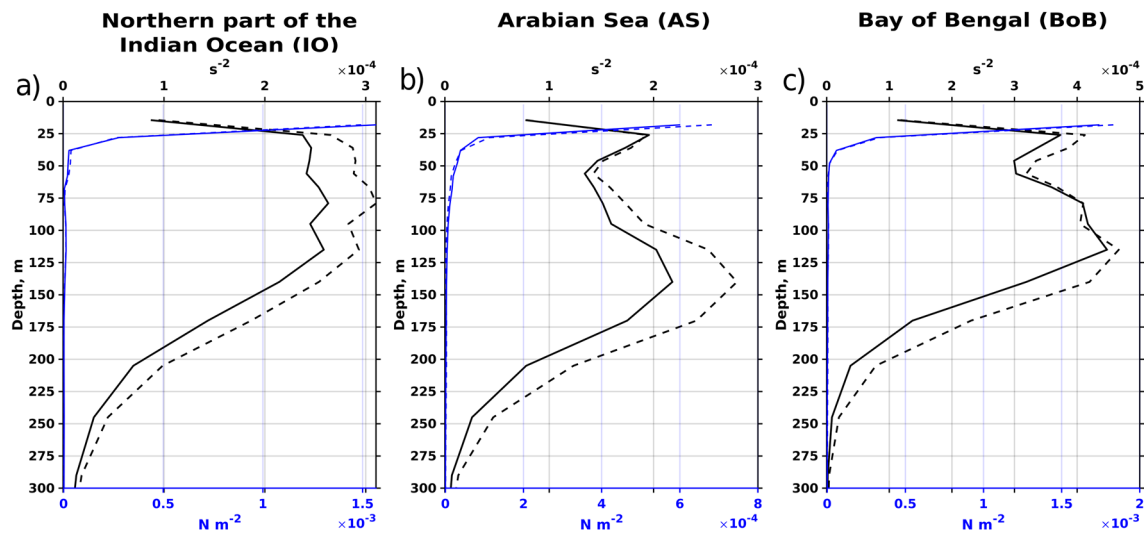


Fig. 5 Vertical profiles of modeled climatic annual-mean Brunt-Väisälä frequency squared (black lines, s^{-2}) and shear stress (blue lines, $N m^{-2}$) for the periods 1975–2004 and 2070–2099 in IO (a), AS (b) and BoB (c). IO denotes the northern part of the Indian

Ocean, AS Arabian Sea, BoB Bay of Bengal (see Fig. 1 for the exact locations of these regions). Solid line is for 1975–2004, dashed line is for 2070–2099

winter (monsoon) season showed corresponding altering of thermal effect of Tibetan Plateau and the role of the changes in the monsoon circulation. It is also noteworthy that the climate signal in the driving MPI-ESM-LR global model does not reflect the importance of orographic features on the climate change signal. Moreover, MPI-ESM-LR simulates strong warming over the Indian subcontinent, which can be related to the low resolution of its atmospheric component ECHAM6 (Giorgetta et al. 2013).

The SST differences between the corresponding seasons of the two climatic periods reached more than $3.4\text{ }^{\circ}\text{C}$ in the AS. The minimum differences between the two climatic periods in the AS occurred in the pre-monsoon period (MAM) and were equal to $2.7\text{--}2.9\text{ }^{\circ}\text{C}$ on average. Therefore, the future SST increase in the BoB will be less pronounced than in the AS, being about $2.8\text{ }^{\circ}\text{C}$ annually, but reaching $3.0\text{--}3.4\text{ }^{\circ}\text{C}$ during the winter and pre-monsoon period, and decreasing to $2.2\text{--}2.4\text{ }^{\circ}\text{C}$ during the post-monsoon period (ON).

During the summer monsoon period, the southwestern winds carry relatively cool sea air from the ocean towards India. As a result, significant SST deviations will occur along the coasts of Somalia and the Arabian Peninsula in the future compared to the present climate as seen from the spatial distribution of the 2 m air temperature (T2M) in Figs. 2 and 6. From these figures it is also evident that during the summer monsoon season (JJAS) the air above the Arabian Peninsula and Somalia is strongly warmed. The impact of monsoon transport of the relatively cool air upon the air temperature above India is also seen during the JJAS and ON seasons when the difference between the changes of

air temperature above the ocean and land is minimal in the southern and south-western Indian states.

Considering the biological productivity on a seasonal scale, the widespread decrease of the PP in the future climate is noteworthy, especially pronounced in the northern and western parts of the AS during the monsoon and post-monsoon periods. The model results also showed a significant drop in PP along the western coast of the BoB in the future during the monsoon period. The reason for such a decrease in PP is a MLD decrease, which leads to a decrease in nutrient supply from the deep oceanic layers.

The most pronounced increase of precipitation rate (PR) in the projected future climate occurred over India ($3\text{--}5\text{ mm/day}$) and the eastern coasts of the BoB ($>5\text{ mm/day}$) during the monsoon period, and also over the equatorial band ($2\text{--}3\text{ mm/day}$) during the post-monsoon period (Fig. 7). Although the annual-mean precipitation changes partly reflect the SST warming and the increase in evaporation, different mechanisms are involved in these changes, which depend not only on SST but also include the land-sea gradients and the large-scale circulation. Besides, the spatial patterns of precipitation change are seasonally dependent. For instance, the JJAS precipitation showed two distinct patterns of precipitation change related to the monsoon rain band over land and the Intertropical Convergence Zone (ITCZ) over the ocean, which are dynamically connected through a local Hadley circulation. From Fig. 7, during the monsoon period (JJAS) the rain band over India becomes wetter while the equatorial band becomes weaker, as it is affected by anomalous descending motion and moisture divergence (Hsu et al. 2012). The importance of the changes

Fig. 6 Difference Δ between simulated future (2070–2099) and past (1975–2004) seasonal climatic SST (left column, **a–d**) and T2M (right column, **e–h**). The difference Δ for SST and T2M is statistically significant throughout the study area in all seasons. The statistical significance for the differences was calculated using Student's *t* test at confidence interval of 95%

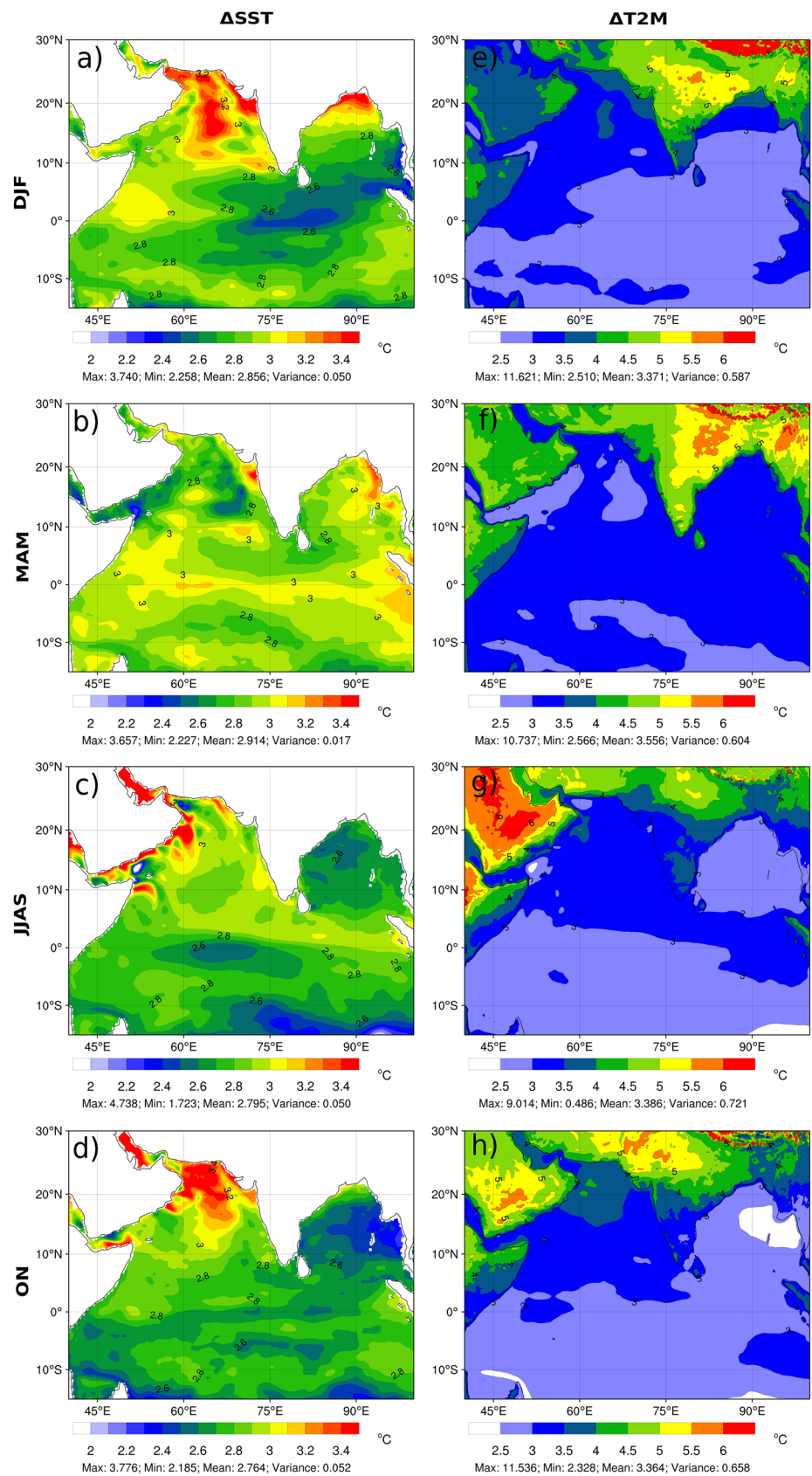


Fig. 7 Difference Δ between simulated future (2070–2099) and past (1975–2004) seasonal climatic PR (left column, **a–d**) and PP (right column, **e–h**). Areas of statistically nonsignificant values are cross-hatched with red lines. The statistical significance for the differences Δ was calculated using Student's *t* test at confidence interval of 95%. In figures where there is no cross-hatching, this means that all values are statistically significant

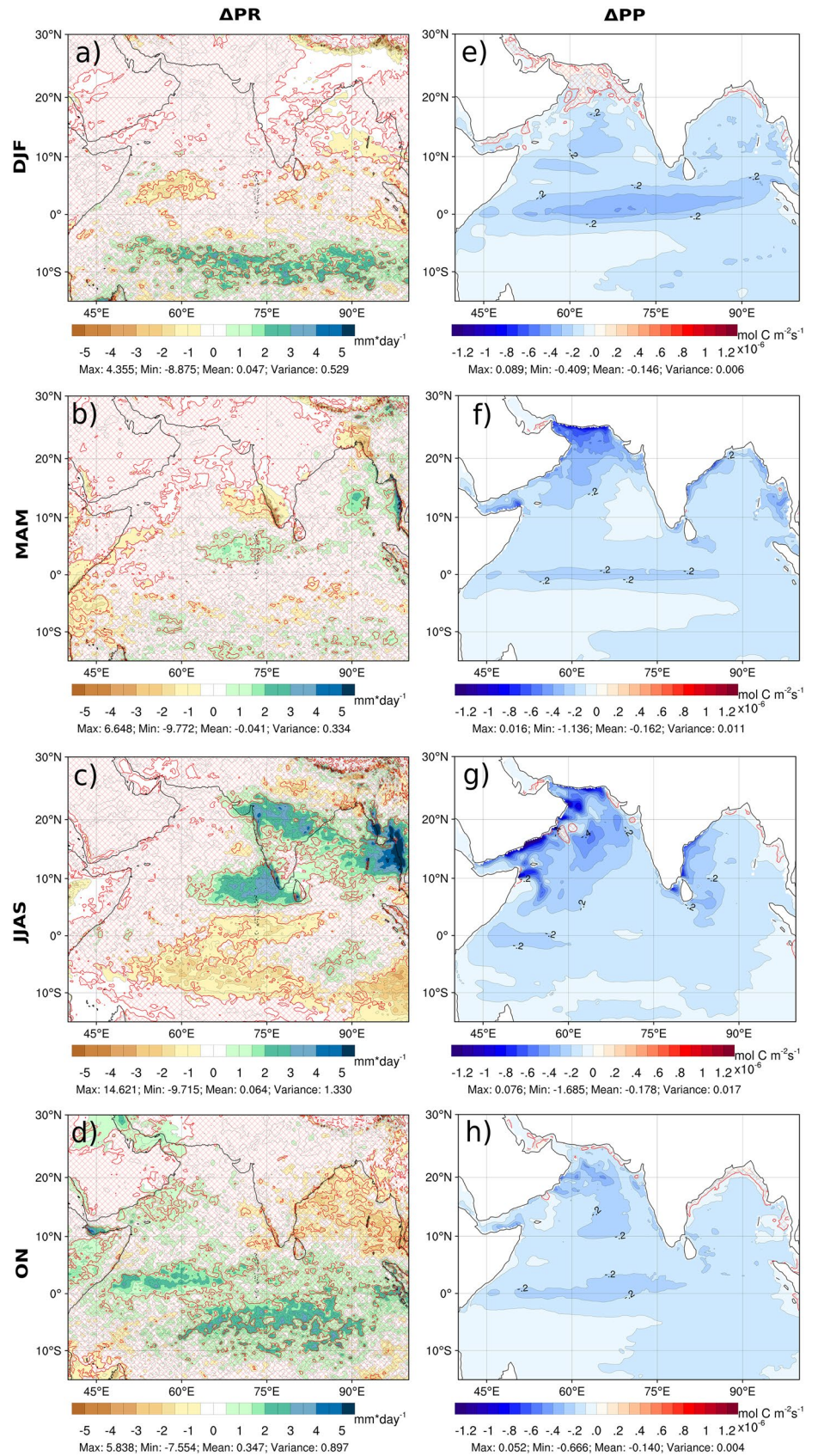
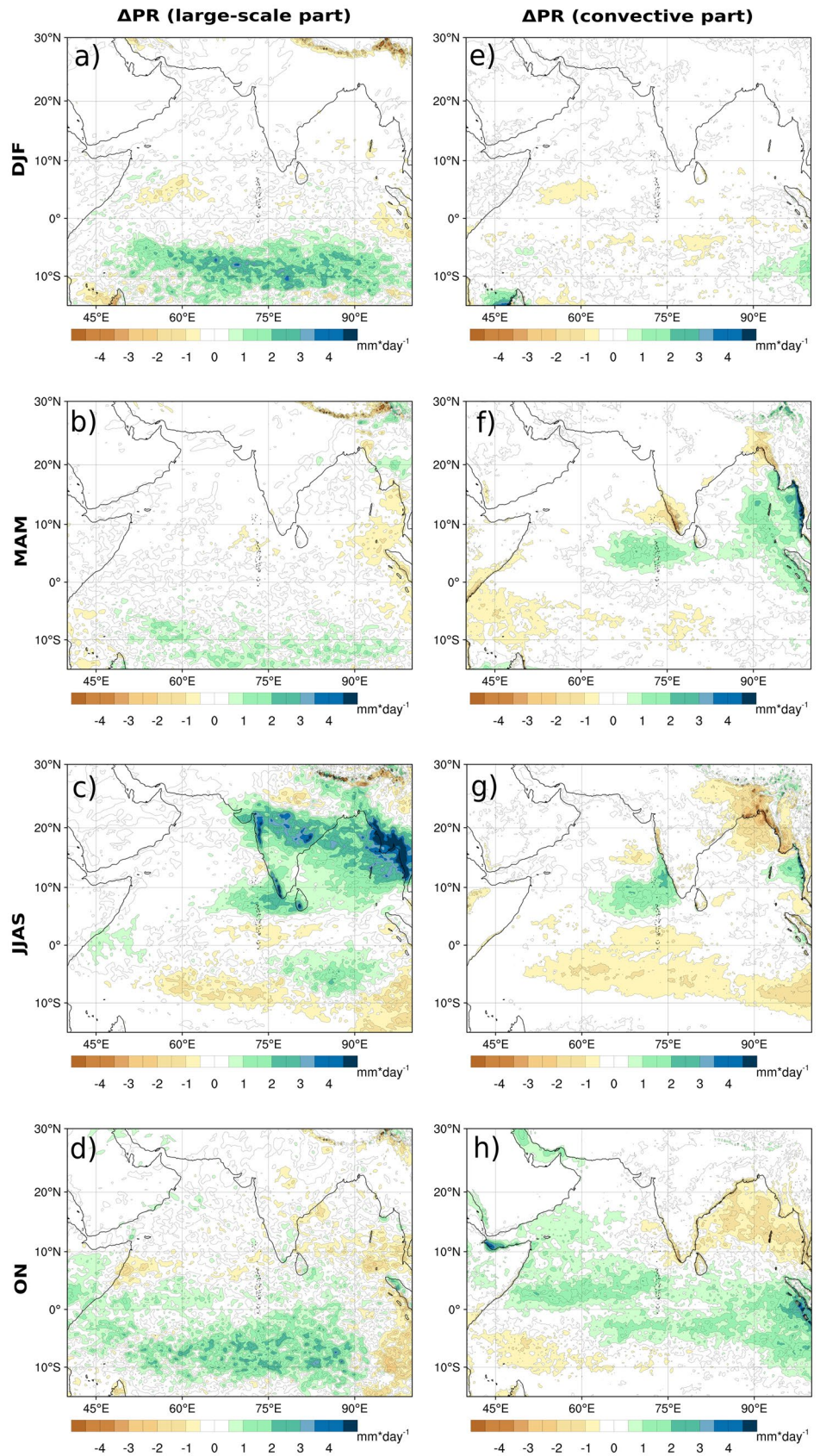


Fig. 8 Difference between simulated future (2070–2099) and past (1975–2004) climatic periods for large-scale (Δ LS, left column, **a–d**) and convective (Δ CONV, right column, **e–h**) components of total precipitation (PR)



in the circulation can be seen in Fig. 8 where we presented the differences between the future and past climatic periods for large-scale (ΔLS) and convective ($\Delta CONV$) components of total precipitation (PR). During both DJF and JJAS climatic seasons, the largest part of the precipitation change was of large-scale nature. It supports the idea that for these seasons, the effect of SST on the precipitation changes mostly took place through changes in the large-scale Hadley circulation.

To assess the changes in the annual climatic monthly-mean behavior of the selected variables, we also analyzed their cycle for the regions considered. From Fig. 9 it is more clearly seen that the spatially-averaged monthly-mean climatic SST in the northern Indian Ocean region will be 2–3 °C higher in the future climate while keeping its climatic intra-annual variability pattern. The same holds for the AS and the BoB regions. The climatic intra-annual variability of 2 m air temperature (T2M) will also replicate this tendency, the difference between the future and past climates being 3–4 °C throughout the year. The surface salinity (SSS) for

the IO and BoB regions will be lower in the future climate than in the past climate, while for the AS region the SSS will increase in the first part of a year and decrease in the second part. This tendency may be explained by the changes of precipitation rates over the considered areas. From Fig. 9, the large drop in SSS in the IO region in October–November may be related to the increase of total precipitation in this region during the same period. This relationship is especially clear for the AS region: the enhancement of PR in July–October leads to the corresponding drop in SSS during the second part of the year. The period of enhanced precipitation over the BoB region in the future climate will also occur in July–October, but the drop in SSS will not be so clear, which can be explained by the strong impact of large river runoff into the BoB shading the influence of atmospheric precipitation.

The decrease of the ocean biological productivity mentioned earlier is also clearly traceable in the intra-annual climatic monthly-mean series of the depth-averaged phytoplankton primary production (PP) averaged over

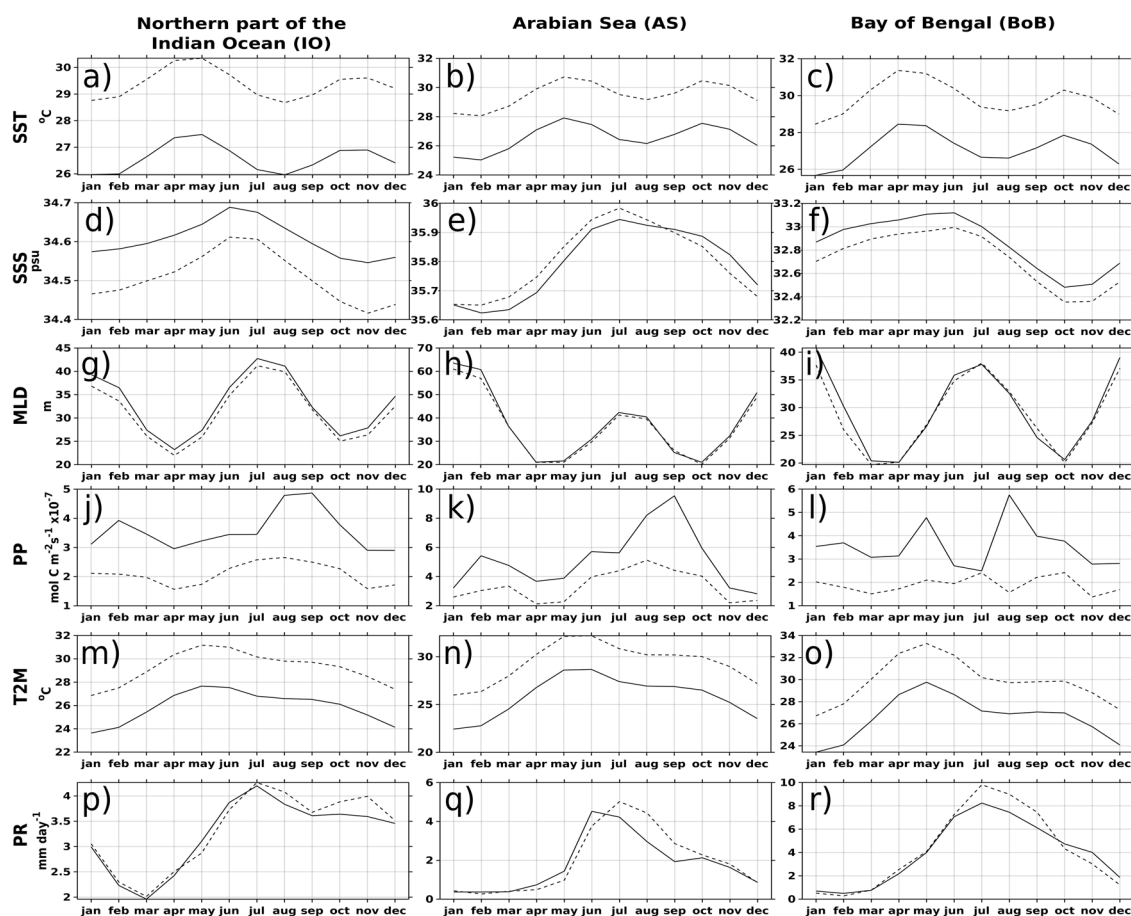


Fig. 9 Modeled annual climatic monthly-mean SST (a–c), SSS (d–f), MLD (g–i), PP (j–l), T2M (m–o) and PR (p–r) for the climatic periods 1975–2004 and 2070–2099. IO denotes the northern part of the

Indian Ocean, AS Arabian Sea, BoB Bay of Bengal (see Fig. 1b for the exact locations of these regions). Solid line is for 1975–2004, dashed line is for 2070–2099

the IO, AS and BoB regions (Fig. 9). According to ROM simulations, none of the considered areas showed an increase of phytoplankton primary production in the future climate. The most significant drop in PP in the future climate compared to the past climate appeared during the monsoon season, i.e., during the annual phytoplankton bloom maximum. The summer phytoplankton bloom in these areas occurs in the monsoon season due to enhanced supply of nutrients from the deeper layers. Thus, the model results suggest that this supply of nutrients will be significantly weakened in the future climate in the northern Indian Ocean. Therefore, according to our simulations, the future climatic intra-annual variability of primary production will be much less pronounced compared to the present. The projected change in MLD is much less noticeable in Fig. 9 compared to the decrease of PP. It may be related to spatial averaging of model results to produce area-mean estimates for IO, AS and BoB. This procedure significantly smooths the fields and conceals any smaller-scale spatial heterogeneity of MLD that may be to some degree responsible for such a decrease in PP on a climatic time-scale. For example, in Fig. 2 the spatial heterogeneity of modeled MLD is obvious. Its largest horizontal gradients are located in the Arabian Sea—a region where the largest simulated PP decrease is also located. Also, the tropical ocean is known to be a region of low nutrient availability for phytoplankton primary production, and therefore a small decrease in nutrient supply from deeper layers due to shallowing of MLD may cause considerable decrease of primary production. We do not discuss this phenomenon in detail in the current study because it deserves a separate study, perhaps even a separate study for each region considered, i.e. for the BoB, AS, or Indian Ocean as a whole, since the global biogeochemical model HAMOCC used in the current study, though capable of catching general patterns of phytoplankton primary production in the global ocean and its parts on a climatic time-scale, may be too coarse to describe a fine-scale processes involving interaction between physical and biogeochemical processes.

4 Comparison of the ROM's projection with other studies

State-of-the-art global climate models are run with spatial resolutions that do not allow for the explicit representation of many features of the regional climate, especially those related to the orographic features over land and to strong air-sea interactions, such as the eastern boundary upwelling systems and western boundary currents. Enclosed seas and surrounding coastal areas, which host a very important part of the human population, are still not very well represented in global models, which are not able to provide detailed climate

information for adaptation and mitigation in these regions (e.g., Kumar et al. 2022a, b; Weber et al. 2023; Soares et al. 2019). The RESM ROM proposed in this study has the advantage of having a rather high spatial resolution (≈ 25 km) that improves the quality of reproduction of climatic characteristics in South Asia, especially the frequency distribution of Indian summer monsoon extremes (Mishra et al. 2022). Besides, there should be confidence about ROM simulations' quality with respect to other available suits of models. Specifically, the historical simulation from ROM should be in good agreement with the available observations. Also, the future projected fields simulated with ROM should be analogous to the projected climate of other models. It should also be emphasized that ROM projections were using CMIP5 forcings (RCP8.5 scenarios) and hence, in order to see the improvement from the use of the regional model ROM and highlight its potential, one should compare its results with other simulations exploiting the same forcing. However, while evaluating the quality of ROM's projections, we must note that a comprehensive quantitative comparison of our projections of all climatic characteristics with their earlier model estimates obtained under the CMIP5 and CMIP6 scenarios, is a separate time-consuming task (e.g., Sharmila et al. 2015) and was not the main goal of our study. Nevertheless, we compared the observed SST, SSS and T2M with the historical simulation of ROM and with its forcing model MPI-ESM-LR (CMIP5) and Multimodel Ensemble mean (MME) of the three best CMIP5 models: MPI-ESM-LR, CMCC-CMS, NorESM1 (Li and Su 2020). This comparison showed better warming trends in the Indian Ocean during the historical period. Also, in order to demonstrate that high-order statistics of ROM are independent of forcing models, we showed that ROM has better performance against the CMIP6 simulation of MPI-ESM-LR (Table 1). To evaluate the performance of ROM, we used the T2M data taken from the ERA5 (Hersbach et al. 2020), as well as the National Oceanic and Atmospheric Administration (NOAA) Optimum Interpolation SST version 2 (OISST.v2) data (Banzon et al. 2016). The simulated SSS was evaluated against the ORAS5 (Zuo et al. 2019) reanalysis. The detailed evaluation of PR was carried out in our previous studies and can be found in (Kumar et al. 2022a, b; Kumari et al. 2022; Mishra et al. 2022a,b).

The projected fields from ROM simulation are in good agreement with the projections from the other models, and we found a strong pattern correlation with all of them (Table 2).

Figure 10 shows spatial fields of SST, SSS and T2M, both observed and simulated with different models including ROM. ROM delineates the region of high and low SST field but with some underestimation, while SSS and T2M fields are well represented in ROM. ROM shows notable discrepancy in terms of SST magnitude, in

Table 1 Performance of ROM and other models against observations for the annual-mean fields during the historical period (1975–2004) for the study area. The observed SST, SSS, and T2M are from OISST, ORAS5, and ERA5.

		ROM	MPI-ESM-LR CMIP5	MME of CMIP5	MPI-ESM-LR CMIP6
SST	Pattern correlation	0.9437	0.9087	0.9228	0.8573
	RMSE	4.4696	5.6195	5.1654	7.4447
	Skill Score	0.3379	0.4248	0.3905	0.5628
SSS	Pattern correlation	0.9402	0.8629	0.9332	0.8729
	RMSE	5.7326	9.0647	6.0749	8.6459
	Skill Score	0.3459	0.547	0.3666	0.5217
T2M	Pattern correlation	0.967	0.9162	0.9121	0.9036
	RMSE	0.8827	1.2385	1.2854	1.4011
	Skill Score	0.2894	0.4061	0.4214	0.4594

Table 2 Pattern correlation of ROM with different models for the annual-mean projected fields during the future period (2070–2099)

	SST	T2M
MPI-ESM-LR CMIP5	0.854	0.8795
MME of CMIP5	0.932	0.8857
MPI-ESM-LR CMIP6	0.8689	0.8461

particular—underestimation over southeast Arabian Sea. The problem is mostly a consequence of a generally cooler simulated SST than that in observations in the Indian Ocean, especially in the equatorial band, in which ROM shows a band of cooler SST in the present-time simulation (Fig. 10). This leads to the presence of the high SST bands over the southeast Arabian Sea and the east equatorial Indian Ocean. This feature is related to the model formulation and,

therefore, appears in the historical period results (Fig. 10), and is also present in the simulation of the future period (Fig. 11). Nevertheless, ROM is able to distinguish most of the regions of low and high SST. For example, the southeast Arabian Sea is a region of high SST in ROM results, which is consistent with observations, attributing to the high correlation (in spite of the cold bias). All other models show good agreement with observations for all parameters. However, the statistics such as pattern correlation, root mean square error (RMSE) and skill score (ratio of RMSE of a model to the standard error of observations) suggest that ROM performs relatively well in comparison with other models (Table 1). ROM has a very high pattern correlation, low RMSE and better skill score (a skill score close to zero represents better model performance). All these facts suggest that ROM has superior performance than its forcing model MPI-ESM-LR from CMIP5 simulations. In addition, based

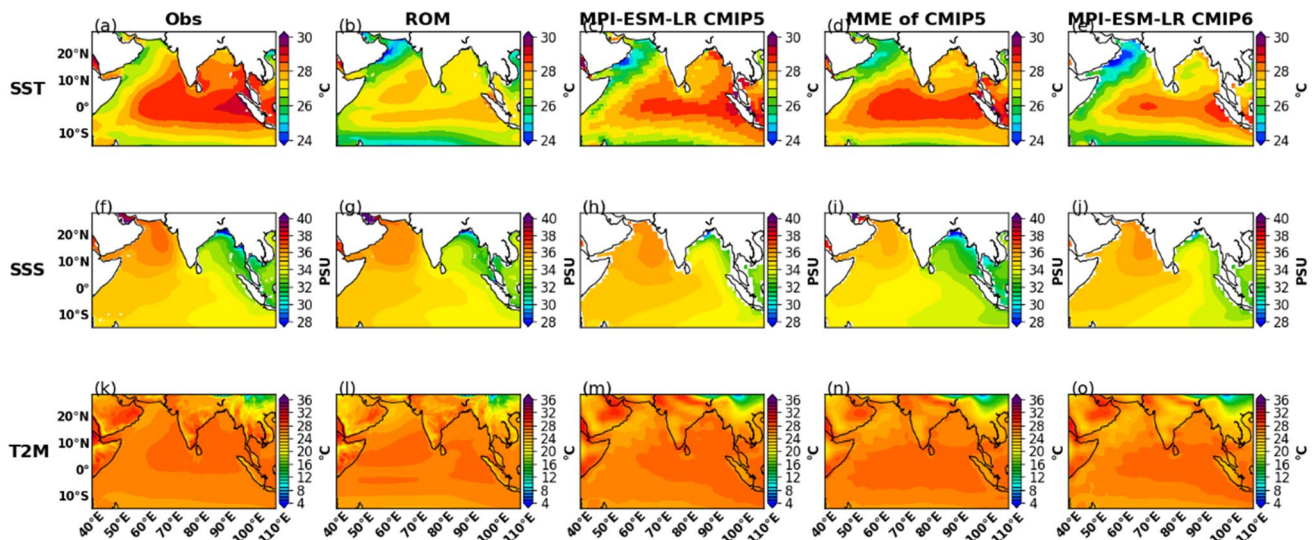


Fig. 10 Performance of ROM, MPI-ESM-LR (CMIP5), MME (CMIP5) and MPI-ESM-LR (CMIP6) against observations for the annual-mean fields for the historical (1975–2004) period. The observed SST (a–e), SSS (f–j) and T2M (k–o) fields are from OISST, ORAS5, and ERA5

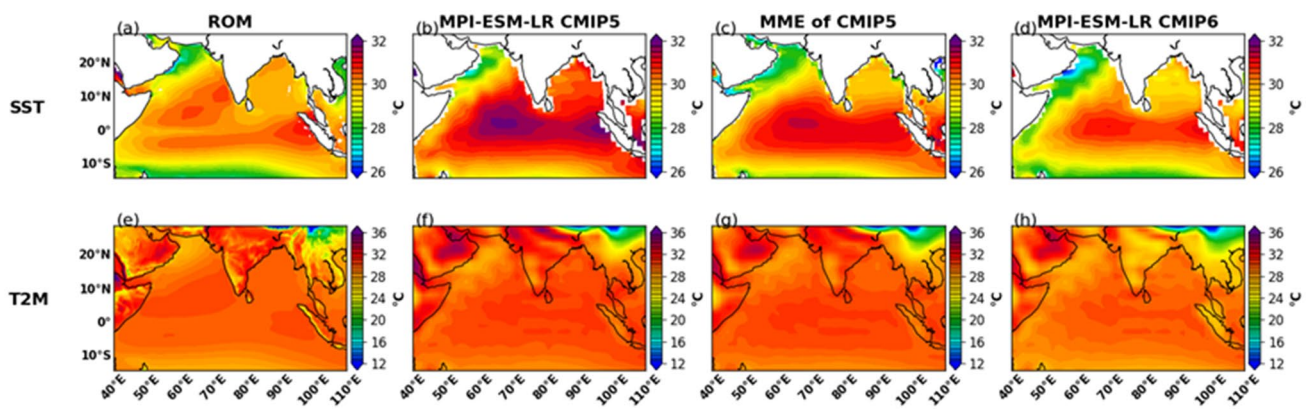


Fig. 11 The similarity between ROM, MPI-ESM-LR (CMIP5), MME (CMIP5) and MPI-ESM-LR (CMIP6) for the annual-mean fields for the future (2070–2099) projected SST (a–d) and T2M (e–h)

on these estimates, ROM outperformed MME from CMIP5 simulations and MPI-ESM-LR from CMIP6 simulations. This advocates the suitability of RESM ROM at a regional scale.

Figure 11 presents the comparison between ROM-projected fields and MPI-ESM-LR (CMIP5), MME (CMIP5) and MPI-ESM-LR (CMIP6) projected fields. We note a good spatial agreement between the results with slight systematic high/low values, although there is a very high pattern correlation (Table 2). The future projection of SST spatial distribution is more or less similar to the historical SST distribution. The similarity between the present-time and future spatial SST patterns is seen in ROM as well as in CMIP5 and CMIP6 models. For example, ROM is relatively colder in the historical simulations than other models, which is the case in future projection as well, making the change (future–past) comparable in all, further confirming feasible climate simulation (no climate drift) in ROM results. Summarizing, the presented modeling framework of ROM over CORDEX South Asia region and corresponding results show the potential for climate change studies and numerous other studies using this model setup, and support the model's suitability (Dubey and Kumar 2023; Kumar et al. 2022a, b; Kumari and Kumar 2023; Mishra et al. 2021; Saharwardi et al. 2021; Sein et al. 2022;).

All estimates made for various characteristics of future precipitation change for the area under consideration referred to the land (e.g., Almazroui et al. 2020; Gupta et al. 2020; Katzenberger et al. 2021) and can be compared with the present work only qualitatively. For example, Katzenberger et al. (2021) performed an analysis of 32 models of the CMIP6 with regard to their annual-mean monsoon rainfall for the land area with latitudes 6–36° N and longitudes 67.5–98° E, comprising India and neighboring regions. They showed that all of those models demonstrated a substantial increase in JJAS-mean rainfall

under unabated climate change (the Shared Socioeconomic Pathway 5–8.5). Most models projected that the increase will contribute especially to the precipitation in the Himalaya region and to the northeast of the BoB, as well as the west coast of India. Although our results are related to a much larger region including the AS, the BoB, the equatorial Indian Ocean, and the southwestern Asian land area, they are in qualitative agreement with these estimates: (1) there is a substantial increase in JJAS rainfall (Fig. 7); (2) the greatest increase in precipitation occurs in the northeastern BoB and on land to the northeast of it, as well as on the west coast of India and the adjoining southeastern part of the AS (Fig. 7). A significant increase in precipitation is also observed in the central part of India. In the Himalayas, there is an intermittent pattern of local increase/decrease in precipitation, with apparently some total predominance being the increase of precipitation.

Adequate comparison of the projected changes in the precipitation extremes over India during the Indian summer monsoon, obtained from the ROM simulations used in this study, with the results of similar studies was performed recently by Kumari and Kumar (2023). Precipitation extremes were computed for India and its six homogeneous regions and subregions of the Western Ghats and central India for the far-future (2070–2099: FRF) with respect to the historical period (1969–2000). In that study, ROM showed better resemblance with observations in simulating precipitation extremes than three other RESMs that participated in the CORDEX-CORE simulation. The intense rainfall (95th percentile: R95) is expected to be enhanced over most of the region during FRF except central northeast and northeast India. Besides, it turned out that long wet (dry) events were shortened (lengthened). This is attributed to the strong cyclonic circulation, reduced vertical wind shear and enhanced moisture transport during the Indian summer monsoon.

The spatial pattern of the precipitation climate change signal in the northern part of the BoB in our model is of opposite sign than in the CMIP5 ensemble-mean presented in Fig. 1 of Li et al. (2017) and in the CMIP6 ensemble-mean presented in Chen et al. (2022). However, as stated in both papers, model biases can be strongly influenced by systematic biases. When corrections are imposed to these simulations, the precipitation climate change signal is reduced and can even change its sign. For instance, the spatial pattern of the precipitation change in our study in the northern part of the BoB is similar to the corrected mean precipitation presented in Fig. 2 of Li et al. (2017). The correction is related to the excess precipitation bias in the present-day simulation over the tropical western Pacific, which affects the circulation in the Indian summer monsoon. This indicates that ROM can adequately capture the cloud–radiation feedback on SST, as proposed by Li et al. (2017). However, it is the decrease in convective precipitation that leads to the future reduction in precipitation. This could be related to an increase in stability.

The comparison of simulated precipitation with other models should be carried out with caution. Regional climate impacts depend on the atmospheric circulation, and individual climate models can show patterns of atmospheric circulation change that can be qualitatively different. The multi-model mean projection could be a likely candidate for such a comparison. However, multi-model ensembles cannot be interpreted in a probabilistic sense (Knutti et al.

2013). Therefore, the uncertainty in the future response must be taken into account when comparing our results with the projections from other models, especially with global ones. To reduce these uncertainties, regional climate change can be analyzed using storylines of atmospheric circulation (Zappa and Shepherd 2017), which essentially group models based on the minimization of the uncertainties related to the main large-scale drivers of the regional climate. Also, the regional model results are influenced by the large-scale circulation of the forcing model, MPI-ESM-LR in our case.

We also compared the future changes in the surface currents pattern obtained with ROM with surface currents changes produced in CMIP5 and CMIP6 simulations. More specifically, we investigated the future changes in the magnitude of surface currents for the Annual, JJAS and ON seasons using MPI-ESM-LR (CMIP5), MME (CMIP5) and MPI-ESM-LR (CMIP6) over the BoB. However, these models are configured at relatively coarse horizontal resolution and hence may have spatial gaps in coastal regions. In contrast, ROM was optimized to work at higher horizontal resolution $0.22^\circ \times 0.22^\circ$ and thus largely got around this issue. Figure 12 shows the difference between simulated future (2070–2099) and historical (1975–2004) seasonal-mean climatic surface currents calculated from the aforementioned CMIP5 and CMIP6 simulations.

These results demonstrate that surface currents will be stronger in the projected future JJAS season. In Annual and ON seasons in the future climate, some areas of the BoB

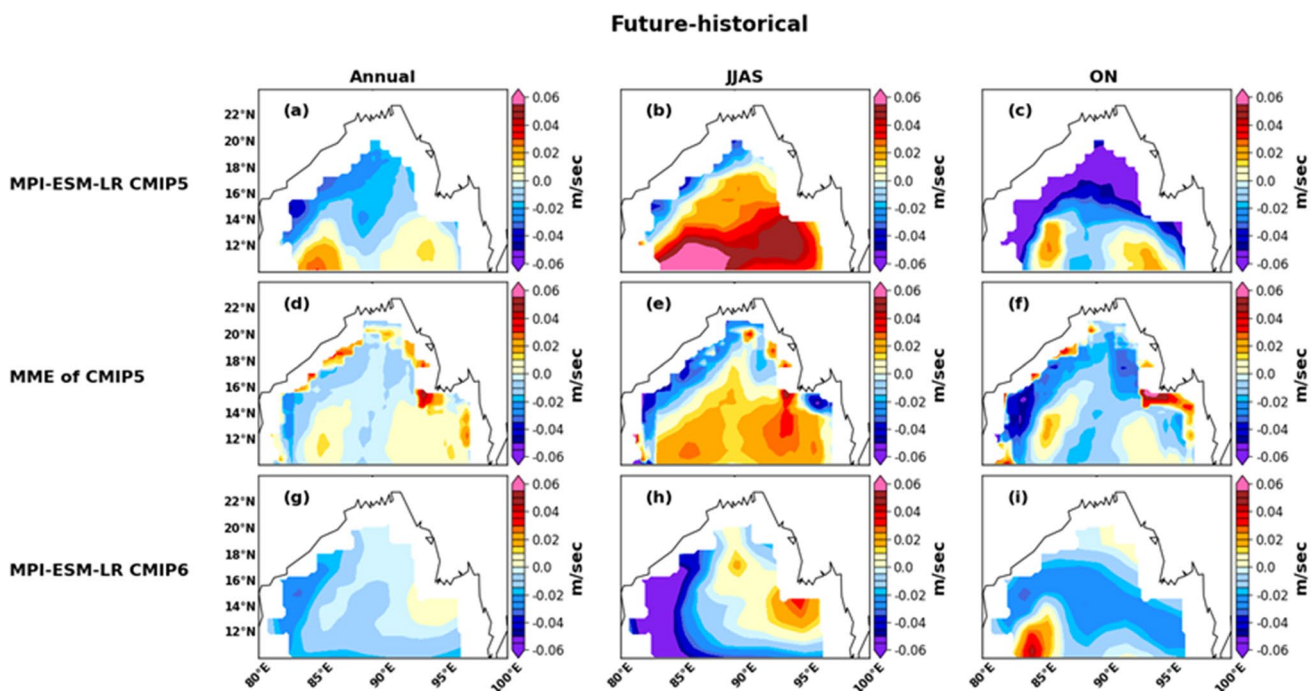


Fig. 12 Difference between simulated future (2070–2099) and historical (1975–2004) climatic surface currents magnitude for the Annual, JJAS and ON seasons in the MPI-ESM-LR (CMIP5) (a–c), MME (CMIP5) (d–f) and MPI-ESM-LR (CMIP6) (g–i) models

will see strengthening while others will see weakening in the strength of surface currents. We do acknowledge that the spatial pattern of changes in the surface current magnitude in the ROM results (Fig. 3) may vary from the patterns displayed by other models (Fig. 12). These discrepancies might be caused by the different model resolution, fully spatio-temporal changing of light attenuation coefficient by marine biogeochemistry in ROM, different parameterizations used in these models, etc. However, exploring all such reasons was not a goal of this study. By mentioning the changes in future currents' pattern in the northern BoB, we want to draw the attention of interested researchers to a more detailed study of possible causes of SSS future changes in that region, which are currently not given much attention. As a rule, SSS changes are associated with variations in precipitation and evaporation in the ice-free open sea, as well as changes in river run-off in coastal areas. In the current study, we showed that coastal circulation features can also have a significant impact on coastal SSS changes in the Bay of Bengal even with relatively small changes in river run-off, thus raising the importance of adequate simulation of coastal ocean circulation, which is known to be highly dependent on a model's horizontal resolution. This circumstance should be taken into account when comparing our results with those produced with CMIP5 or CMIP6 models, choosing only those models that have the same or better horizontal resolution in the study area. However, such a comparison and, more importantly, corresponding analysis and clarification of the causes of various discrepancies between different simulations, remains a difficult task (e.g., Chassignet et al. 2020).

5 Conclusion

The present study aims to assess the future changes in the ocean-atmosphere system in the South Asia region using the high-resolution RESM ROM, which consists of a global ocean model dynamically coupled with a regional atmospheric model. A simulation taking into account the impact of marine biogeochemical variability's feedback on South Asia climate has been carried out for the period 1920–2099. The comparison between the simulated past (1975–2004) and future (2070–2099) climate periods for South Asia CORDEX domain, with a focus on spatial distributions of SST, SSS, depth-integrated phytoplankton primary production, 2 m air temperature, and total precipitation rate is presented. Both climatic annual-mean and seasonal-mean distributions of these parameters are discussed.

We found that the SST in the northern part of the Indian Ocean in the future climate will be significantly higher. At the same time, ocean biological productivity will decrease

compared to the past climate. In the northern part of the Indian Ocean, the average annual SST increase will reach 2.7–3.2 °C by the end of this century, with the annual-mean SST increase reaching 3.4 °C in the northern part of the AS and in the Persian Gulf, SST changes being significant throughout the study area with 95% confidence level. Both water temperature and salinity changes in the future climate will lead to enhanced water stratification and vertical stability of the upper ocean layers, thus hindering the vertical turbulent mixing and nutrient supply to the surface, which results in decreasing of the ocean phytoplankton primary production in the northern part of the Indian Ocean.

The 2 m air temperature will rise significantly in the future, especially above land. Considering the annual-mean pattern, the increase reaches up to 5.5 °C in northern India and Arabian Peninsula, while it is 2.5–3.5 °C over the northern Indian Ocean. The warming during the winter season will be stronger over southern Asia, reaching 7 °C over the northern side of the Himalayas and the Tibetan Plateau. The opposite occurs in the monsoon season. The amount of annual-mean precipitation will substantially increase over the eastern coast of the Bay of Bengal (up to 1.5–2.0 mm/day) and along the equator in the band 10° S – 10° N (0.5–1.5 mm/day), while it will decrease over the western part of the Bay of Bengal and in the northern states of India (–0.5 to 1.0 mm/day). The most pronounced increase of precipitation rate in the future climate will occur over India (3–5 mm/day) and the eastern coasts of the Bay of Bengal (> 5 mm/day) during the monsoon period, and over the equatorial band (2–3 mm/day) during the post-monsoon period, with all precipitation changes indicated above being significant at 95% confidence level.

The model results suggest that the surface currents' pattern in the northern part of the BoB will intensify in the future climate, with two gyres of the opposite rotation direction being one of features of this new circulation pattern. Their combined effect leads to the local circulation that to some degree traps the waters freshened by the riverine runoff in the top of the BoB by means of the recirculation of that water.

The finding of this study can be further extended to explore the ocean extremes, hazards, the marine ecosystem, and long-lasting biological impacts. They also could be useful for addressing changing coastal risks from sea-level rise and build a regional framework over the Indian Ocean for climate services focused on assisting decision-makers. Furthermore, since our model setup consists of the physical environment and interactions between the marine ecosystem, it can be used for the extended assessment of the future of ecosystem components which can be helpful to guide better management strategies.

The Indian Ocean has a tremendous potential fishing zone. Thus, the reliable high-resolution projected ocean

parameter can be used to explore the migration of marine species, in particular fish, and it can potentially contribute to improving the management of marine living resources and climate services to provide the foundation for an informed decision-making.

Acknowledgements AKM and PK were supported by the Department of Science and Technology (DST), Govt. of India (Grant No. DST/INT/RUS/RSF/P-33/G). DVS, SDM, AYD and VAR worked in the framework of the SIO RAS state assignment (No. FMWE-2021-0014). DVS was also supported by the Federal Ministry of Education and Research of Germany (BMBF) in the framework of ACE project (Grant 01LP2004A). WC was funded by the Alcalá University project (PIUAH21/CC-058) and the Spanish Ministry of Science, Innovation and Universities, through grant (I+D+I PID2021-128656OB-I00) This work used resources of the Deutsches Klimarechenzentrum (DKRZ) granted by its Scientific Steering Committee (WLA) under project ID ba1144. We thank anonymous reviewers for constructive suggestions and comments.

Author contributions DS and SM wrote the main manuscript text. DS did the model simulations. AD, VR, AM, WC, NL, AL, DJ, PK did data analysis. AD, AL prepared the figures. All authors reviewed the manuscript.

Funding Open Access funding enabled and organized by Projekt DEAL.

Data availability (Data transparency). Model forcing data and observational data are freely available, model output data can be downloaded from https://swift.dkrz.de/v1/dkrz_ffd3ca9004324ad28243244b834f92b1/Indian_future/Data_for_Future_Climate_Change_in_the_Northern_Indian_Ocean.zip?temp_url_sig=4068d83fbc9e516012ea5ea75b21a7c002c62cd6&temp_url_expires=2028-10-09T11:04:01Z.

The ERA5 data (Hersbach et al. 2020) can be obtained from <https://www.ecmwf.int/en/forecasts/datasets/reanalysis-datasets/era5>. The OISST data (Banzon et al. 2016) can be downloaded from National Centers for Environmental Information (NCEI) in Network Common Data Form (netCDF) at <https://doi.org/10.7289/V5SQ8XB5>. The ORAS5 data (Zuo et al. 2019) can be obtained from <https://cds.climate.copernicus.eu/cdsapp#!/dataset/reanalysis-oras5>.

Code availability (Software application or custom code). The model codes of ROM and REMO can be requested from the Alfred Wegener Institute for Polar and Marine Research and the Climate Service Center Germany (GERICS). Scripts for data processing are stored in an internal GitLab, software used are bash scripts, CDO and Python.

Declarations

Conflict of interest Authors do not have any conflict interests or competing interests to declare.

Open Access This article is licensed under a Creative Commons Attribution 4.0 International License, which permits use, sharing, adaptation, distribution and reproduction in any medium or format, as long as you give appropriate credit to the original author(s) and the source, provide a link to the Creative Commons licence, and indicate if changes were made. The images or other third party material in this article are included in the article's Creative Commons licence, unless indicated otherwise in a credit line to the material. If material is not included in the article's Creative Commons licence and your intended use is not permitted by statutory regulation or exceeds the permitted use, you will need to obtain permission directly from the copyright holder. To view a copy of this licence, visit <http://creativecommons.org/licenses/by/4.0/>.

References

- Almazroui M, Saeed S, Saeed F, Islam MN, Ismail M (2020) Projections of precipitation and temperature over the south asian countries in CMIP6. *Earth Syst Environ* 4:297–320. <https://doi.org/10.1007/s41748-020-00157-7>
- Banzon V, Smith TM, Chin T M, Liu C, Hankins W (2016) A long-term record of blended satellite and in situ sea-surface temperature for climate monitoring, modeling and environmental studies. *Earth Syst Sci Data* 8:165–176. <https://doi.org/10.5194/essd-8-165-2016>
- Beal LM, Vialard J, Roxy MK, Lead authors (2019) Executive summary. IndOOS-2: a road map to sustained observations of the Indian Ocean for 2020–2030. CLIVAR-4/2019, GOOS-237, p 8. <https://doi.org/10.36071/clivar.rp.4-1.2019>
- Bopp L, Resplandy L, Orr JC, Doney SC, Dunne JP, Gehlen M, Halloran P, Heinze C, Ilyina T, Séférian R, Tjiputra J, Vichi M (2013) Multiple stressors of ocean ecosystems in the 21st century: projections with CMIP5 models. *Biogeosciences* 10:6225–6245. <https://doi.org/10.5194/bg-10-6225-2013>
- Chassignet EP, Yeager SG, Fox-Kemper B, Bozec A, Castruccio F, Danabasoglu G, Horvat C, Kim WM, Koldunov N, Li Y, Lin P, Liu H, Sein DV, Sidorenko D, Wang Q, Xu X (2020) Impact of horizontal resolution on global ocean–sea ice model simulations based on the experimental protocols of the Ocean Model Intercomparison Project phase 2 (OMIP-2). *Geosci Model Dev* 13:4595–4637. <https://doi.org/10.5194/gmd-13-4595-2020>
- Chen Z, Zhou T, Chen X, Zhang W, Zhang L, Wu M, Zou L (2022) Observationally constrained projection of afro-asian monsoon precipitation. *Nat Commun* 13:2552. <https://doi.org/10.1038/s41467-022-30106-z>
- Di Sante F, Coppola E, Farneti R, Giorgi F (2019) Indian summer monsoon as simulated by the regional earth system model RegCM-ES: the role of local air–sea interaction. *Clim Dyn* 53:759–778. <https://doi.org/10.1007/s00382-019-04612-8>
- Dubey AK, Kumar P (2023) Future projections of heatwave characteristics and dynamics over India using a high-resolution regional earth system model. *Clim Dyn* 60:127–145. <https://doi.org/10.1007/s00382-022-06309-x>
- Giorgetta MA, Jungclaus J, Reick CH, Legutke S, Bader J, Böttinger M, Brovkin V, Crueger T, Esch M, Fieg K, Glushak K, Gayler V, Haak H, Hollweg H-D, Ilyina T, Kinne S, Kornblüeh L, Matei D, Mauritsen T, Mikolajewicz U, Mueller W, Notz D, Pithan F, Raddatz T, Rast S, Redler R, Roeckner E, Schmidt H, Schnur R, Segschneider J, Six KD, Stockhause M, Timmreck C, Wegner J, Widmann H, Wieners K-H, Claussen M, Marotzke J, Stevens B (2013) Climate and carbon cycle changes from 1850 to 2100 in MPI-ESM simulations for the coupled model intercomparison project phase 5: climate changes in MPI-ESM. *J Adv Model Earth Syst* 5:572–597. <https://doi.org/10.1002/jame.20038>
- Gröger M, Maier-Reimer E, Mikolajewicz U, Moll A, Sein D (2013) NW European shelf under climate warming: implications for open ocean – shelf exchange, primary production, and carbon absorption. *Biogeosciences* 10:3767–3792. <https://doi.org/10.5194/bg-10-3767-2013>
- Guo Y, Cao J, Li H, Wang J, Ding Y (2016) Simulation of the interface between the indian summer monsoon and the east asian summer monsoon: intercomparison between MPI-ESM and ECHAM5/MPI-OM. *Adv Atmos Sci* 33:294–308. <https://doi.org/10.1007/s00376-015-5073-z>
- Gupta V, Singh V, Jain MK (2020) Assessment of precipitation extremes in India during the 21st century under SSP1-1.9 mitigation scenarios of CMIP6 GCMs. *J Hydrol* 590:125422. <https://doi.org/10.1016/j.jhydrol.2020.125422>

- Hagemann S, Dümenil L (1997) A parametrization of the lateral water flow for the global scale. *Clim Dyn* 14:17–31. <https://doi.org/10.1007/s003820050205>
- Hersbach H, Bell B, Berrisford P et al (2020) The ERA5 global reanalysis. *Q J R Meteorol Soc* 146:1999–2049. <https://doi.org/10.1002/qj.3803>
- Hossain MM, Anwar AF, Garg N, Prakash M, Bari M (2022) Evaluation of CMIP5 decadal precipitation at catchment level. <https://doi.org/10.21203/rs.3.rs-2245410/v1>
- Hsu P-C, Li T (2012) Is rich-get-richer valid for Indian Ocean and Atlantic ITCZ? *Geophys Res Lett* 39:L13705
- Ilyina T, Six KD, Segschneider J, Maier-Reimer E, Li H, Núñez-Riboni I (2013) Global ocean biogeochemistry model HAM-OCC: model architecture and performance as component of the MPI-Earth system model in different CMIP5 experimental realizations. *J Adv Model Earth Syst* 5:287–315. <https://doi.org/10.1029/2012MS000178>
- Jacob D (2001) A note to the simulation of the annual and inter-annual variability of the water budget over the Baltic Sea drainage basin. *Meteorol Atmos Phys* 77:61–73. <https://doi.org/10.1007/s007030170017>
- Jensen TG (2001) Arabian Sea and Bay of Bengal exchange of salt and tracers in an ocean model. *Geophys Res Lett* 28:3967–3970. <https://doi.org/10.1029/2001GL013422>
- Jerlov NG (1976) *Marine optics*. Elsevier oceanography series, vol 14. Elsevier Scientific Pub. Co, Amsterdam ; New York
- Jungclauss JH, Fischer N, Haak H, Lohmann K, Marotzke J, Matei D, Mikolajewicz U, Notz D, Storch JS (2013) Characteristics of the ocean simulations in the Max Planck Institute Ocean Model (MPIOM) the ocean component of the MPI-Earth system model. *J Adv Model Earth Syst* 5:422–446. <https://doi.org/10.1002/jame.20023>
- Katzenberger A, Schewe J, Pongratz J, Levermann A (2021) Robust increase of indian monsoon rainfall and its variability under future warming in CMIP6 models. *Earth Syst Dyn* 12:367–386. <https://doi.org/10.5194/esd-12-367-2021>
- Knutti R, Masson D, Gettelman A (2013) Climate model genealogy: generation CMIP5 and how we got there. *Geophys Res Lett* 40:1194–1199. <https://doi.org/10.1002/grl.50256>
- Koné V, Aumont O, Lévy M, Resplandy L (2009) Physical and biogeochemical controls of the phytoplankton seasonal cycle in the Indian Ocean: a modeling study. In: Wiggert JD, Hood RR, Naqvi SWA, Brink KH, Smith SL (eds) *Geophysical Monograph Series*. American Geophysical Union, Washington, pp 147–166. <https://doi.org/10.1029/2008GM000700>
- Krishnan R, Sanjay J, Gnanaseelan C, Mujumdar M, Kulkarni A, Chakraborty S (eds) (2020) *Assessment of Climate Change over the Indian Region: a report of the Ministry of Earth Sciences (MoES), government of India*. Springer Singapore, Singapore. <https://doi.org/10.1007/978-981-15-4327-2>
- Kumar P, Mallick S, Mishra AK, Dubey AK, Tiwari G, Sein DV, Cabos W, Jacob D (2022a) Regional earth system model for CORDEX-South Asia: a comparative assessment of RESM and ESM over the tropical Indian Ocean. *Int J Climatol* 42(16):9131–9149. <https://doi.org/10.1002/joc.7806>
- Kumar P, Mishra AK, Dubey AK, Javed A, Saharwardi MS, Kumari A, Sachan D, Cabos W, Jacob D, Sein DV (2022b) Regional earth system modelling framework for CORDEX-SA: an integrated model assessment for indian summer monsoon rainfall. *Clim Dyn* 59:2409–2428. <https://doi.org/10.1007/s00382-022-06217-0>
- Kumari A, Kumar P (2023) Evaluation and future projection of the extreme precipitation over India and its homogeneous regions: a Regional Earth System Model Perspective. *Int J Climatol*. <https://doi.org/10.1002/joc.8052>
- Lakku NK, Behera MR (2022) Skill and inter-model comparison of regional and global climate models in simulating wind speed over south Asian domain. *Climate* 10(6):85. <https://doi.org/10.3390/cli10060085>
- Laufkötter C, Vogt M, Gruber N, Aita-Noguchi M, Aumont O, Bopp L, Buitenhuis E, Doney SC, Dunne J, Hashioka T, Hauck J, Hirata T, John J, Le Quéré C, Lima ID, Nakano H, Seferian R, Totterdell I, Vichi M, Völker C (2015) Drivers and uncertainties of future global marine primary production in marine ecosystem models. *Biogeosciences* 12:6955–6984. <https://doi.org/10.5194/bg-12-6955-2015>
- Li J, Su J (2020) Comparison of Indian Ocean warming simulated by CMIP5 and CMIP6 models. *Atmos Ocean Sci Lett* 13(6):604–611. <https://doi.org/10.1080/16742834.2020.1824546>
- Li T, Zhang Y, Lu E, Wang D (2002) Relative role of dynamic and thermodynamic processes in the development of the Indian Ocean dipole: an OGCM diagnosis: dynamic and thermodynamic processes. *Geophys Res Lett* 29:25-1–25-4. <https://doi.org/10.1029/2002GL015789>
- Li G, Xie S-P, He C, Chen Z (2017) Western Pacific emergent constraint lowers projected increase in indian summer monsoon rainfall. *Nat Clim Change* 7:708–712. <https://doi.org/10.1038/nclimate3387>
- Luo J-J, Masson S, Behera S, Yamagata T (2007) Experimental forecasts of the Indian Ocean dipole using a coupled OAGCM. *J Clim* 20:2178–2190. <https://doi.org/10.1175/JCLI4132.1>
- Marsland SJ, Haak H, Jungclauss JH, Latif M, Röske F (2003) The Max-Planck-Institute global ocean/sea ice model with orthogonal curvilinear coordinates. *Ocean Model* 5:91–127. [https://doi.org/10.1016/S1463-5003\(02\)00015-X](https://doi.org/10.1016/S1463-5003(02)00015-X)
- McCreary JP, Kundu PK, Molinari RL (1993) A numerical investigation of dynamics, thermodynamics and mixed-layer processes in the Indian Ocean. *Prog Oceanogr* 31:181–244. [https://doi.org/10.1016/0079-6611\(93\)90002-U](https://doi.org/10.1016/0079-6611(93)90002-U)
- McSweeney CF, Jones RG, Lee RW, Rowell DP (2015) Selecting CMIP5 GCMs for downscaling over multiple regions. *Clim Dyn* 44:3237–3260. <https://doi.org/10.1007/s00382-014-2418-8>
- Mishra AK, Dwivedi S, Di Sante F (2021a) Performance of the RegCM-MITgcm coupled regional model in simulating the Indian summer Monsoon Rainfall. *Pure Appl Geophys* 178:603–617. <https://doi.org/10.1007/s00024-020-02648-0>
- Mishra AK, Kumar P, Dubey AK, Javed A, Saharwardi MS, Sein DV, Martyanov SD, Jacob D (2021b) Impact of horizontal resolution on monsoon precipitation for CORDEX-South Asia: a regional earth system model assessment. *Atmos Res* 259:105681. <https://doi.org/10.1016/j.atmosres.2021.105681>
- Mishra AK, Dubey AK, Dinesh AS (2022) Diagnosing whether the increasing horizontal resolution of regional climate model inevitably capable of adding value: investigation for indian summer monsoon. *Clim Dyn*. <https://doi.org/10.1007/s00382-022-06424-9>
- Narvekar J, Prasanna Kumar S (2014) Mixed layer variability and chlorophyll a biomass in the Bay of Bengal. *Biogeosciences* 11:3819–3843. <https://doi.org/10.5194/bg-11-3819-2014>
- Paulson CA, Simpson JJ (1977) Irradiance measurements in the Upper Ocean. *J Phys Oceanogr* 7:952–956. [https://doi.org/10.1175/1520-0485\(1977\)007%3c0952:IMITUO%3e2.0.CO;2](https://doi.org/10.1175/1520-0485(1977)007%3c0952:IMITUO%3e2.0.CO;2)
- Phillips HE, Tandon A, Furue R, Hood R, Ummenhofer CC, Benthuisen JA, Menezes V, Hu S, Webber B, Sanchez-Franks A, Cherian D, Shroyer E, Feng M, Wijesekera H, Chatterjee A, Yu L, Hermes J, Murtugudde R, Tozuka T, Su D, Singh A, Centurioni L, Prakash S, Wiggert J (2021) Progress in understanding of Indian Ocean circulation, variability, air–sea exchange, and impacts on biogeochemistry. *Ocean Sci* 17:1677–1751. <https://doi.org/10.5194/os-17-1677-2021>

- Purwaningsih A, Hidayat R (2016) Performance of decadal prediction in coupled model intercomparison project phase 5 (CMIP5) on projecting climate in tropical area. *Procedia Environ Sci* 33:128–139. <https://doi.org/10.1016/j.proenv.2016.03.064>
- Ratnam JV, Giorgi F, Kaginalkar A, Cozzini S (2009) Simulation of the indian monsoon using the RegCM3–ROMS regional coupled model. *Clim Dyn* 33:119–139. <https://doi.org/10.1007/s00382-008-0433-3>
- Roxy MK, Modi A, Murtugudde R, Valsala V, Panickal S, Prasanna Kumar S, Ravichandran M, Vichi M, Lévy M (2016) A reduction in marine primary productivity driven by rapid warming over the tropical Indian Ocean. *Geophys Res Lett* 43:826–833. <https://doi.org/10.1002/2015GL066979>
- Saharwardi MS, Kumar P, Sachan D (2021) Evaluation and projection of drought over India using high-resolution regional coupled model ROM. *Clim Dyn* 58:503–521. <https://doi.org/10.1007/s00382-021-05919-1>
- Samala BK, Banerjee CN, Kaginalkar S, Dalvi A (2013) Study of the indian summer monsoon using WRF–ROMS regional coupled model simulations: indian summer monsoon using WRF–ROMS regional coupled model. *Atmos Sci Lett* 14:20–27. <https://doi.org/10.1002/asl2.409>
- Schott FA, Xie S-P, McCreary JP (2009) Indian Ocean circulation and climate variability. *Rev Geophys* 47:RG1002. <https://doi.org/10.1029/2007RG000245>
- Sein DV, Mikolajewicz U, Gröger M, Fast I, Cabos W, Pinto JG, Hagemann S, Semmler T, Izquierdo A, Jacob D (2015) Regionally coupled atmosphere–ocean–sea ice–marine biogeochemistry model ROM: 1. Description and validation. *J Adv Model Earth Syst* 7:268–304. <https://doi.org/10.1002/2014MS000357>
- Sein DV, Dvornikov AY, Martyanov SD, Cabos W, Ryabchenko VA, Gröger M, Mishra AK, Kumar P, Gorchakov VA (2021) Influence of the water temperature–phytoplankton feedback on the upper layer temperature of the Indian Ocean. *Fundam Prikl Hidrofiz* 14:64–76. <https://doi.org/10.7868/S2073667321040067>
- Sein DV, Dvornikov AY, Martyanov SD, Cabos W, Ryabchenko VA, Gröger M, Jacob D, Kumar Mishra A, Kumar P (2022) Indian Ocean marine biogeochemical variability and its feedback on simulated South Asia climate. *Earth Syst Dyn* 13:809–831. <https://doi.org/10.5194/esd-13-809-2022>
- Sengupta D, Bharath Raj GN, Shenoi SSC (2006) Surface freshwater from Bay of Bengal runoff and Indonesian throughflow in the tropical Indian Ocean. *Geophys Res Lett* 33:L22609. <https://doi.org/10.1029/2006GL027573>
- Sharmila S, Joseph S, Sahai AK, Abhilash S, Chattopadhyay R (2015) Future projection of Indian summer monsoon variability under climate change scenario: an assessment from CMIP5 climate models. *Glob Planet Change* 124:62–78. <https://doi.org/10.1016/j.gloplacha.2014.11.004>
- Shaw R, Luo Y, Cheong TS, Abdul Halim S, Chaturvedi S, Hashizume M, Insarov GE, Ishikawa Y, Jafari M, Kitoh A, Pulhin J, Singh C, Vasant K, Zhang Z (2022) Asia. In: Pörtner O, Roberts DC, Tignor M, Poloczanska ES, Mintenbeck K, Alegría A, Craig M, Langsdorf S, Löschke S, Möller V, Okem A, Rama B (eds) *Climate Change 2022: impacts, adaptation and vulnerability. Contribution of Working Group II to the Sixth Assessment Report of the Intergovernmental Panel on Climate Change*. H. Cambridge University Press, Cambridge, pp 1457–1579. <https://doi.org/10.1017/9781009325844.012>
- Shen Y, Sun Y, Zhong Z, Li T (2021) A quantitative method to evaluate the performance of climate models in simulating global tropical cyclones. *Front Earth Sci* 9:693934. <https://doi.org/10.3389/feart.2021.693934>
- Sillmann J, Kharin VV, Zhang X, Zwiers FW, Bronaugh D (2013) Climate extremes indices in the CMIP5 multimodel ensemble: part 1. Model evaluation in the present climate. *J Geophys Res: Atmos* 118(4):1716–1733. <https://doi.org/10.1002/jgrd.50203>
- Soares PMM, Lima DC, Semedo A, Cabos W, Sein DV (2019) Climate change impact on Northwestern African offshore wind energy resources. *Environ Res Lett* 14:124065
- Sperber KR, Annamalai H, Kang I-S, Kitoh A, Moise A, Turner A, Wang B, Zhou T (2013) The Asian summer monsoon: an intercomparison of CMIP5 vs. CMIP3 simulations of the late century. *Clim Dyn* 41:2711–2744. <https://doi.org/10.1007/s00382-012-1607-6>
- Srivastava A, Dwivedi S, Mishra AK (2018) Investigating the role of air–sea forcing on the variability of hydrography, circulation, and mixed layer depth in the Arabian Sea and Bay of Bengal. *Oceanologia* 60:169–186. <https://doi.org/10.1016/j.oceano.2017.10.001>
- Steinacher M, Joos F, Frölicher TL, Bopp L, Cadule P, Cocco V, Doney SC, Gehlen M, Lindsay K, Moore JK, Schneider B, Segsneider J (2010) Projected 21st century decrease in marine productivity: a multi-model analysis. *Biogeosciences* 7:979–1005. <https://doi.org/10.5194/bg-7-979-2010>
- Supari S, Tangang F, Juneng L, Cruz F, Chung JX, Ngai ST, Salimun E, Mohd MSF, Santisirisonboon J, Singhruck P, Phan Van T, Ngo-Duc T, Narisma G, Aldrian E, Gunawan D, Sopaheluwakan A (2020) Multi-model projections of precipitation extremes in Southeast Asia based on CORDEX–Southeast Asia simulations. *Environ Res* 184:109350. <https://doi.org/10.1016/j.envres.2020.109350>
- Tangang F, Chung JX, Juneng L, Supari, Salimun E, Ngai ST, Jamaluddin AF, Mohd MSF, Cruz F, Narisma G, Santisirisonboon J, Ngo-Duc T, Van Tan P, Singhruck P, Gunawan D, Aldrian E, Sopaheluwakan A, Grigory N, Remedio ARC, Sein DV, Hein-Griggs D, McGregor JL, Yang H, Sasaki H, Kumar P (2020) Projected future changes in rainfall in Southeast Asia based on CORDEX–SEA multi-model simulations. *Clim Dyn* 55:1247–1267. <https://doi.org/10.1007/s00382-020-05322-2>
- UNISDR (2016) *Poverty & death: disaster mortality 1996–2015*. Centre for Research on the Epidemiology of Disasters, https://www.unisdr.org/files/50589_credidastermortalityallfinalpdf.pdf
- Vázquez-Patiño A, Campozano L, Mendoza D, Samaniego E (2020) A causal flow approach for the evaluation of global climate models. *Int J Climatol* 40(10):4497–4517. <https://doi.org/10.1002/joc.6470>
- Vinayachandran PN, Iizuka S, Yamagata T (2002) Indian Ocean dipole mode events in an ocean general circulation model. *Deep Sea Res Part II* 49:1573–1596. [https://doi.org/10.1016/S0967-0645\(01\)00157-6](https://doi.org/10.1016/S0967-0645(01)00157-6)
- Weber T, Cabos W, Sein DV, Jacob D (2023) Benefits of simulating precipitation characteristics over Africa with a regionally-coupled atmosphere–ocean model. *Clim Dyn* 60:1079–1102. <https://doi.org/10.1007/s00382-022-06329-7>
- Wiggert JD, Murtugudde RG, Christian JR (2006) Annual ecosystem variability in the tropical Indian Ocean: results of a coupled biophysical ocean general circulation model. *Deep Sea Res Part II* 53:644–676. <https://doi.org/10.1016/j.dsr2.2006.01.027>
- Zappa G, Shepherd TG (2017) Storylines of atmospheric circulation change for European regional climate impact assessment. *J Clim* 30:6561–6577. <https://doi.org/10.1175/JCLI-D-16-0807.1>
- Zheng X-T, Xie S-P, Vecchi GA, Liu Q, Hafner J (2010) Indian Ocean Dipole response to global warming: analysis of ocean–atmospheric feedbacks in a coupled model*. *J Clim* 23:1240–1253. <https://doi.org/10.1175/2009JCLI3326.1>
- Zuo H, Balmaseda MA, Tietsche S, Mogensen K, Mayer M (2019) The ECMWF operational ensemble reanalysis–analysis system for ocean and sea ice: a description of the system and assessment. *Ocean Sci* 15:779–808. <https://doi.org/10.5194/os-15-779-2019>